

# The Atmosphere of Uranus (Oxford Research Encyclopedia of Planetary Science)

LEIGH N. FLETCHER <sup>1</sup>

<sup>1</sup>*School of Physics and Astronomy, University of Leicester, University Road, Leicester, LE1 7RH, United Kingdom.*

## ABSTRACT

Uranus provides a unique laboratory to test our understanding of planetary atmospheres under extreme conditions. Multi-spectral observations from Voyager, ground-based observatories, and space telescopes have revealed a delicately banded atmosphere punctuated by storms, waves, and dark vortices, evolving slowly under the seasonal influence of Uranus' extreme axial tilt. Condensables like methane and hydrogen sulphide play a crucial role in shaping circulation, clouds, and storm phenomena via latent heat release through condensation, strong equator-to-pole gradients suggestive of equatorial upwelling and polar subsidence, and through forming stabilising layers that may decouple different circulation and convective regimes as a function of depth. Phase transitions in the watery depths may also decouple Uranus' atmosphere from motions within the interior. Weak vertical mixing and low atmospheric temperatures associated with Uranus' negligible internal heat means that stratospheric methane photochemistry occurs in a unique high-pressure regime, decoupled from the influx of external oxygen. The low homopause also allows for the formation of an extensive ionosphere. Finally, the atmosphere provides a window on the bulk composition of Uranus - the ice-to-rock ratio, supersolar elemental and isotopic enrichments inferred from remote sensing and future *in situ* measurements - providing key insights into its formation and subsequent migration.

This review reveals the state of our knowledge of the time-variable circulation, composition, meteorology, chemistry, and clouds on this enigmatic 'Ice Giant,' summarising insights from more than three decades of observations, and highlighting key questions for the next generation of planetary missions. As a cold, hydrogen-dominated, intermediate-sized, slowly-rotating, and chemically-enriched world, Uranus could be our closest and best example of atmospheric processes on a class of worlds that may dominate the census of planets beyond our own Solar System.

*Keywords:* Ice Giants, Atmospheres, Uranus, Dynamics, Meteorology, Chemistry, Clouds

Contents			
1. Introduction	2	3.1.3. Composition Contrasts	9
2. Observations of Uranus	2	3.1.4. Meridional Overturning	10
2.1. A Brief Observational History	2	3.2. Uranian Meteorology	10
2.2. Vertical Structure and Composition	4	3.2.1. Convective Storms	10
3. Atmospheric Processes	7	3.2.2. Discrete Cloud Activity	11
3.1. Atmospheric Circulation	7	3.2.3. Vortices and Waves	12
3.1.1. Planetary Banding	7	3.3. Chemistry	12
3.1.2. Winds and Temperatures	7	3.3.1. Methane Photochemistry	12
		3.3.2. Coupling to External Oxygen	13
		3.3.3. Radiative Balance	14
		3.4. Temporal Change	14
		3.5. Connections	15
		3.5.1. Connection to the Interior	15
		3.5.2. Connection to the Exterior	16
		4. Conclusions and Outstanding Questions	16

## 1. INTRODUCTION

Of all the primary planets in our Solar System, Uranus could be considered as the most unusual. Knocked onto its side, potentially by a cataclysmic impact during the epoch of planetary formation and migration (Safronov 1966; Stevenson 1986; Kegerreis et al. 2019), the  $98^\circ$  axial tilt subjects the atmosphere to extreme seasons, with each pole spending four decades in the darkness of polar winter, and four decades in perpetual sunlight. Unlike the other giants, Uranus lacks any detectable internal heat source emanating from its deep interior (i.e., no appreciable ‘self luminosity,’ Pearl et al. 1990), which may be related to the apparent dearth of large-scale meteorological activity and atmospheric mixing. The sluggish vertical mixing results in stratospheric chemistry operating in a higher-pressure regime quite unlike that found on other worlds. Compared to the Gas Giants Jupiter and Saturn, Uranus (and Neptune) possess substantial super-solar enrichments in heavy elements, such that the resulting volatiles (methane, hydrogen sulphide, ammonia, and water) play a crucial role in the stability and energetics of the weather layer. These gaseous species exhibit strong equator-to-pole gradients, hinting at large-scale tropospheric circulation. Combined with the smaller size (4.2 Earth radii), slower rotation (17 hours), and colder tropospheric temperatures ( $\sim 50$  K, sufficient for methane to condense) compared to the Gas Giants, these factors all have stark implications for Uranus’ banded structure, circulation, meteorology, and photochemistry. Indeed, Uranus’ atmosphere occupies a unique region of dynamical and chemical parameter space not found elsewhere in our Solar System.

Uranus therefore provides a planetary-scale laboratory to test our understanding of atmospheric physics and chemistry under extreme environmental conditions. Comparison to Neptune, the archetype for a seasonal Ice Giant, reveals how planets can evolve down different evolutionary paths despite their common origins, allowing us to contrast the extreme seasons and negligible internal heat flux of tilted Uranus with the ever-changing storms of Neptune. Taken together, the Ice Giants are our closest and best examples of a class of ‘intermediate-sized’ astrophysical object that may be common in our universe. Indeed, they are only slightly larger than the sub-Neptunes that dominate the current exoplanetary census (Fulton and Petigura 2018). Exploration of Uranus and Neptune therefore reveals how atmospheric circulation, planetary banding, and seasonal photochemistry operate on cold, intermediate-sized, chemically-enriched, and slow-rotating hydrogen-rich worlds (Fletcher et al. 2020b; Wakeford and Dalba 2020). Finally, the basic composition of Uranus - its ice-

to-rock ratio, supersolar elemental enrichment, and isotopic composition - provides an essential missing piece in the puzzle of the architecture of our Solar System, revealing the location and timescale for Uranus’ accretion (Mousis et al. 2018), and providing insights into its subsequent migration and thermal evolution.

More than 35 years have now passed since the only spacecraft to visit Uranus, Voyager 2, flew past in 1986 on its journey out of our Solar System. Our knowledge of Ice Giant atmospheres was reviewed shortly after the Voyager encounters by Lunine (1993). Since then, observations from ground- and space-based observatories have revealed a picture of Uranus’ atmosphere that is complex, perplexing, and altogether unlike that seen on the Gas Giants. The reader is directed to several recent reviews that investigate aspects of Uranus’ atmosphere in great depth: the bulk composition and implications for planetary origins (Mousis et al. 2018; Atreya et al. 2020); the meteorology (Hueso and Sánchez-Lavega 2019; Hueso et al. 2020), global circulation (Fletcher et al. 2020a), and electrical influences (Aplin et al. 2020) on Uranus’ troposphere; stratospheric chemistry (Moses et al. 2020); and upper atmospheric structure (Melin 2020). Looking to the future, Uranus’ atmosphere will be a key target for future orbital and *in situ* exploration, alongside in depth studies of the interior, magnetosphere, rings and icy satellites (Arridge et al. 2012; Mousis et al. 2018; Hofstadter et al. 2019; Fletcher et al. 2020b).

This article attempts to create a synthesis of these works to review the current state of our understanding of this enigmatic world. Section 2 provides a brief observational history of Uranus, and describes the basic properties of its atmosphere. Section 3 then explores our knowledge of Uranus’ circulation, meteorology, and chemistry, revealing how the atmosphere may be connected to both the deep, hidden, water-rich interior, and the charged environment of the magnetosphere. We will conclude in Section 4 with the significant outstanding questions that must be addressed by future missions to this extreme Ice Giant.

## 2. OBSERVATIONS OF URANUS

### 2.1. *A Brief Observational History*

Although the colourful cloud patterns of Jupiter and Saturn had been intensely studied for centuries, Uranus’ atmosphere remained stubbornly out of reach. Faint dusky belts were suggested as early as 1883 by Young, and 1884 by the Henrys (Young 1883; Henry and Henry 1884), and can be seen in drawings (Alexander 1965) by G. Fournier (1913) and R.L. Waterfield (1915-16). As Uranus was at autumn equinox (planetocentric so-

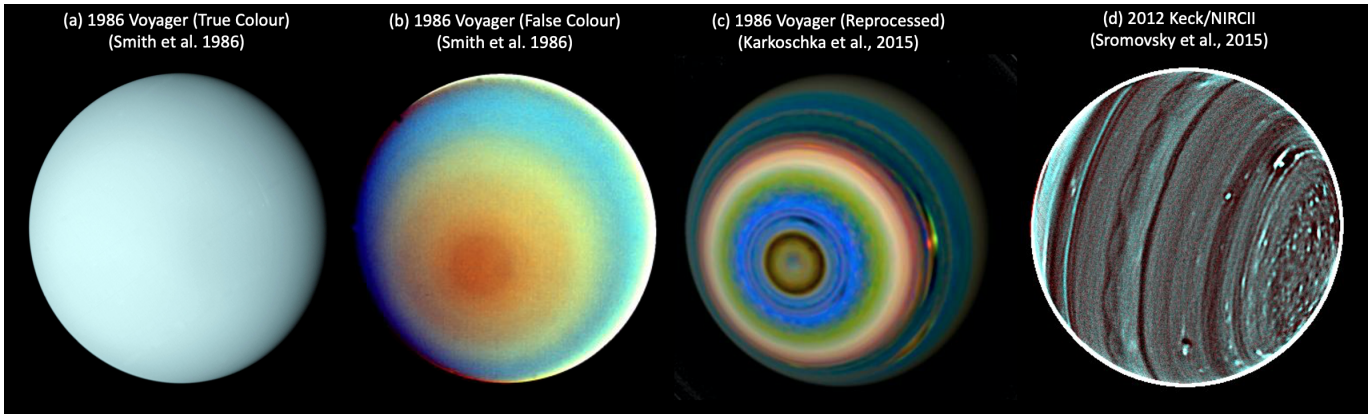


**Figure 1.** Evolution of Uranus observations from Voyager (a-c) to ground-based observatories (d). Uranus originally appeared rather featureless in Voyager-2 observations (Smith et al. 1986) despite attempts to stretch the contrast (b). Modern image processing techniques (c) reveal more structure (Karkoschka 2015), but longer-wavelength observations and derotation techniques (e.g., Keck H-band images in 2012, Sromovsky et al. 2015) are one of the best ways to investigate the details of the atmosphere.

lar longitude,  $L_s = 180^\circ$ ) in 1882, and spring equinox ( $L_s = 0^\circ$ ) in 1923, both hemispheres would have been visible at these times, but the curious orientations of the sketched bands left their existence in doubt. Using spectroscopy, Slipher (1904) discovered dark bands in the visible spectrum which were later demonstrated to be signatures of methane (Wildt 1932). Furthermore, spectral features identified by Kuiper (1949) were found to be due to molecular hydrogen (Herzberg 1952), such that the basic atmospheric composition (a hydrogen atmosphere enriched in methane) was known long before the space age.

The secrets of Uranus’ atmosphere only really started to be revealed by Voyager 2 encounter on 1986-01-24 as part of its ‘Grand Tour,’ and this 1970s spacecraft remains the only mission to ever provide close up views (Smith et al. 1986; Lindal et al. 1987; Tyler et al. 1986). At the time of the flyby, Uranus was just past northern winter solstice ( $L_s = 271.4^\circ$ ), meaning that the southern polar region was pointing almost directly at the Sun. Visible light images from the Voyager cameras (Smith et al. 1986) in Fig. 1 revealed a greeny-blue world due to the high abundance of red-absorbing methane, with faint banding associated with methane condensation clouds, but very few discrete features - only eight features were available to understand the pattern of zonal winds. Early Hubble observations of Uranus in 1994-1995, during northern winter ( $L_s = 310^\circ$ ) (Karkoschka 1997) were similarly bland, although near-IR images began to provide more contrast in 1997 ( $L_s = 319^\circ$ ) (Karkoschka 1998, 2001a,b). Modern image processing of the Voyager-2 data by Karkoschka (2015) revealed many more southern hemisphere features (Fig. 1c), but the perception of Uranus as a featureless planet had already started to take root, albeit unfairly. Subsequent

Earth-based near-IR imaging (Fig. 1d) exploited strong methane and hydrogen absorption bands in the 1-2.2  $\mu\text{m}$  range (‘red wavelengths’) to improve contrast, sensing the aerosol distribution (condensate clouds and photochemical hazes) as a function of altitude (e.g., Fry et al. 2012; Sromovsky et al. 2015, and others). Uranus passed northern spring equinox ( $L_s = 0^\circ$ ) in December 2007 (Fig. 2), permitting the first views of the north pole as it emerged into sunlight (Sromovsky et al. 2009; de Pater et al. 2011; Sromovsky et al. 2012). Today, modern equipment and image processing techniques now allow amateur observers to track prominent storms and bands on Uranus (de Pater et al. 2015). These visible and near-IR observations are summarised by Hueso and Sánchez-Lavega (2019) and described in Section 3, and started to reveal Uranus’ finely banded structure, bright clouds, vortices, and ephemeral storms in exquisite detail (Fig. 2).

Interpreting aerosol distributions requires an understanding of atmospheric temperature and composition, which requires observations in the mid-IR, far-IR, sub-millimetre and radio (Fig. 2). The extreme cold and distance has severely limited our ability to explore this wavelength domain. Although Voyager 2 carried a capable thermal-IR spectrometer, the radiance was so low that only the hydrogen-helium continuum in the 25-50  $\mu\text{m}$  range could be used, revealing tropospheric temperature contrasts between cold mid-latitudes, associated with upwelling, and the warm equator and pole, potentially due to subsidence (Conrath et al. 1998). Space telescopes like ISO (Encrenaz et al. 2000), Herschel (Feuchtgruber et al. 2013) and Spitzer (Orton et al. 2014a) provided high-quality spectra from the infrared to the sub-mm (Fig. 3), but these were disc-integrated, unable to resolve contrasts across Uranus’ atmosphere.

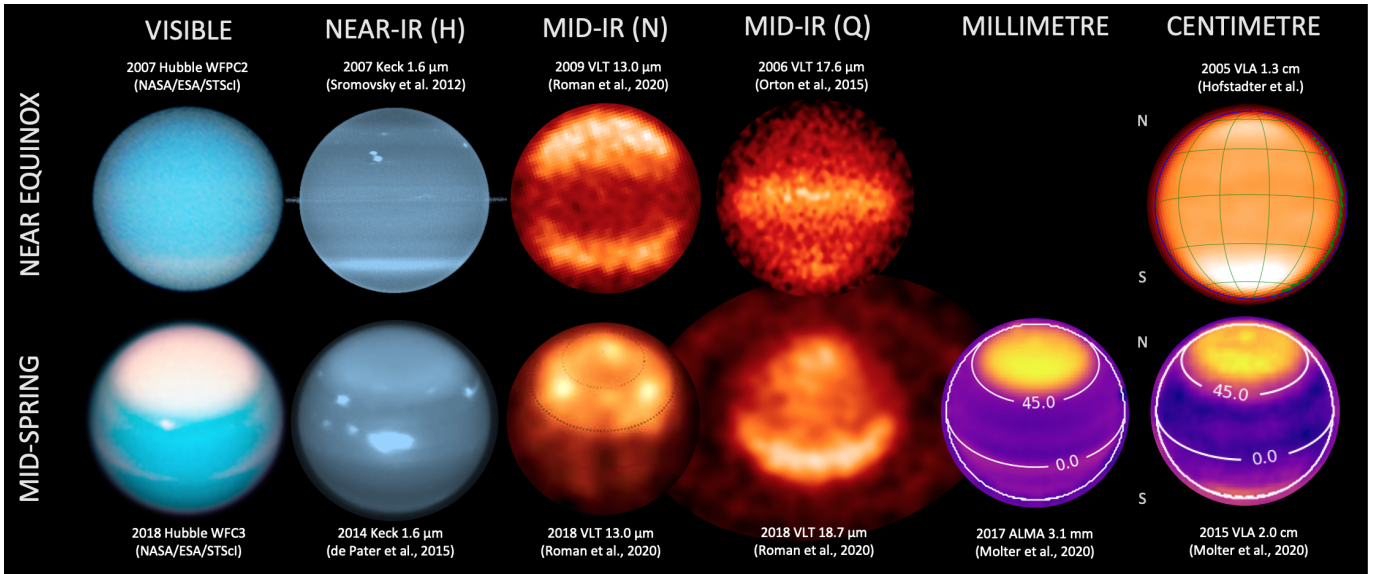


**Figure 2.** Imaging of Uranus from the visible to the radio, in two groups: near the 2007 equinox (top row), and during mid-northern spring (bottom row). From left to right, we show visible-light images from Hubble WFPC2 and WFC3 (Credit: NASA/ESA/STScI); near-infrared images from Keck (Sromovsky et al. 2015; de Pater et al. 2015); mid-IR images of the stratosphere ( $13\ \mu\text{m}$ ) and troposphere ( $18.7\ \mu\text{m}$ ) from VLT (Roman et al. 2020); millimetre observations from ALMA (Molter et al. 2021); and centimetre-wave observations from VLA (Molter et al. 2021). Uranus has been oriented so the the north pole is at the top.

The development of ground-based observatories with  $> 8\text{-m}$  primary mirrors (Keck, VLT, Gemini, and Subaru) now permits spatially-resolved imaging of Uranus’ thermal emission in the  $7\text{-}25\ \mu\text{m}$  range, sensing both tropospheric ( $0.1\text{-}1.0\ \text{bar}$ ) and stratospheric ( $0.1\text{-}10\ \text{mbar}$ ) temperatures (Orton et al. 2015; Roman et al. 2020), albeit with a low signal-to-noise as shown in Fig. 2. Such temperature measurements are supported by occultations of stars in the UV (Bishop et al. 1990). At longer wavelengths, centimetre and millimetre-wavelength arrays like the Karl G. Jansky Very Large Array (VLA) and Atacama Large Millimeter Array (ALMA) (de Pater and Gulkis 1988; Hofstadter and Butler 2003; de Pater et al. 2014) provide maps of gaseous contrasts at greater depths (Fig. 2), with spatial resolutions now approaching those of the reflected-sunlight images (de Pater et al. 2018; Molter et al. 2021). These microwave observations sense thermal emission down to tens of bars, modulated by the pressure-broadened wings of  $\text{NH}_3$  and  $\text{H}_2\text{S}$ , along with other potential contributions from  $\text{CH}_4$ ,  $\text{CO}$ ,  $\text{H}_2\text{O}$ , and  $\text{PH}_3$ , although uniquely distinguishing between these contributions remains a challenge (see (Fig. 3d,) de Pater 1991). Finally, observations of thermospheric emission from  $\text{H}_2$  and  $\text{H}_3^+$  also enable studies of the temperatures and circulation of the upper atmosphere (ionosphere and thermosphere).

Taken together, the observations of reflected sunlight and thermal emission in Fig. 3 are revealing Uranus’

atmosphere in three dimensions, and studying how it evolves over time, as discussed in the following sections.

## 2.2. Vertical Structure and Composition

Before delving into the details of the processes shaping Uranus’ atmosphere, we first review the basic properties of the troposphere and stratosphere, shown in Fig. 4. Based on Uranus’ expected formation region beyond the snowline, the bulk of the planet is thought to be made up of  $10\text{-}20\%$  hydrogen and helium, plus  $80\text{-}90\%$  heavier elements (Hubbard et al. 1995; Podolak et al. 2019). The proportion of rocky refractory materials versus ice-rich materials remains unclear, but the most abundant condensable species are expected to be  $\text{CH}_4$ ,  $\text{H}_2\text{O}$ ,  $\text{NH}_3$ , and  $\text{H}_2\text{S}$ . Of these only  $\text{CH}_4$  and  $\text{H}_2\text{S}$  (Irwin et al. 2018) have been directly measured: methane was first estimated to comprise around  $1.6\text{-}2.3\%$  from Voyager radio occultations (Lindal et al. 1987) and ground-based visible quadrupole measurements (Baines et al. 1995), but later estimates are in the  $2.7\text{-}3.5\%$  range (Karkoschka and Tomasko 2009; Sromovsky et al. 2019). Based on these chemical abundances, and the Clausius-Clapeyron equation (Weidenschilling and Lewis 1973; Sánchez-Lavega et al. 2004), Uranus’ topmost clouds (Fig. 5) are expected to be comprised of a thin layer of  $\text{CH}_4$  ice with a base near  $1.3\ \text{bars}$  and approximately  $80\ \text{K}$ , where latent heat released by condensation was observed to modify the temperature lapse rate observed in Voyager



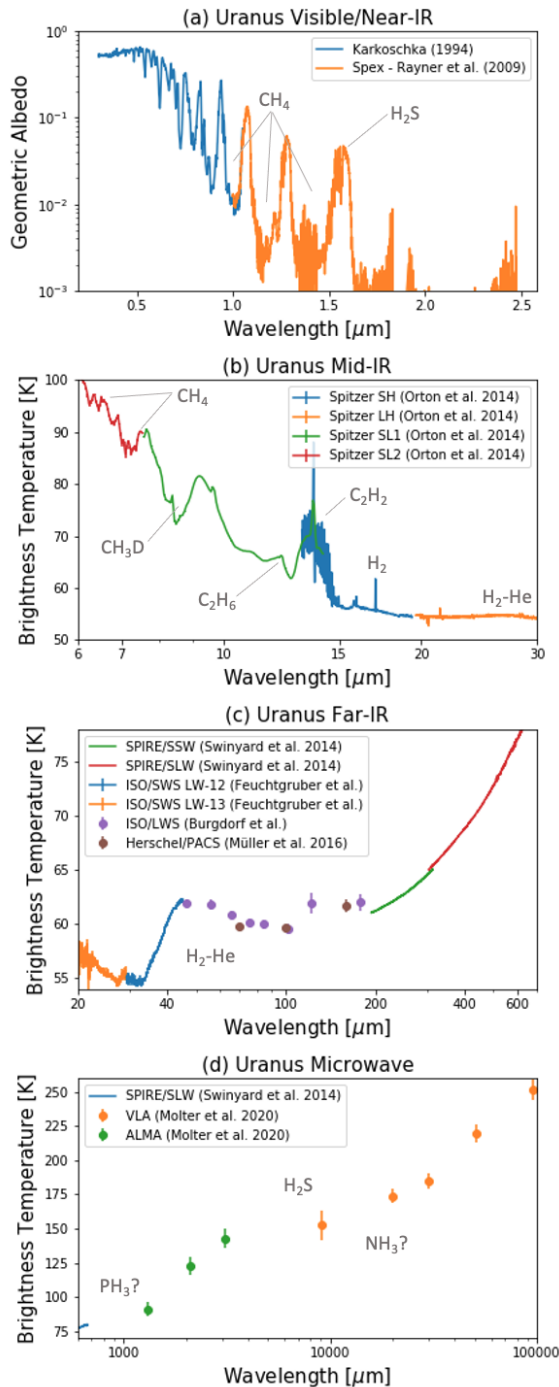


**Figure 3.** Disc-integrated spectroscopy of Uranus from the visible to the radio, with key spectroscopic features labelled. Panel (a) shows reflected sunlight measured by Karkoschka (1994) and Rayner et al. (2009). Panel (b) presents Spitzer/IRS observations of Uranus in low and high-resolution modes (Orton et al. 2014a). Panel (c) reveals the far-IR continuum dominated by collision-induced H<sub>2</sub>-He continuum, constructed from Herschel SPIRE shortwave and longwave spectra (Swinyard et al. 2014) and PACS photometry (Müller et al. 2016), along with ISO Shortwave (courtesy of H. Feuchtgruber) and Longwave (courtesy of M. Burgdorf) spectra. Panel (d) shows VLA and ALMA observations from Molter et al. (2021). Panels (b-d) are presented in brightness temperatures as a proxy for the atmospheric temperatures in the line-formation regions.

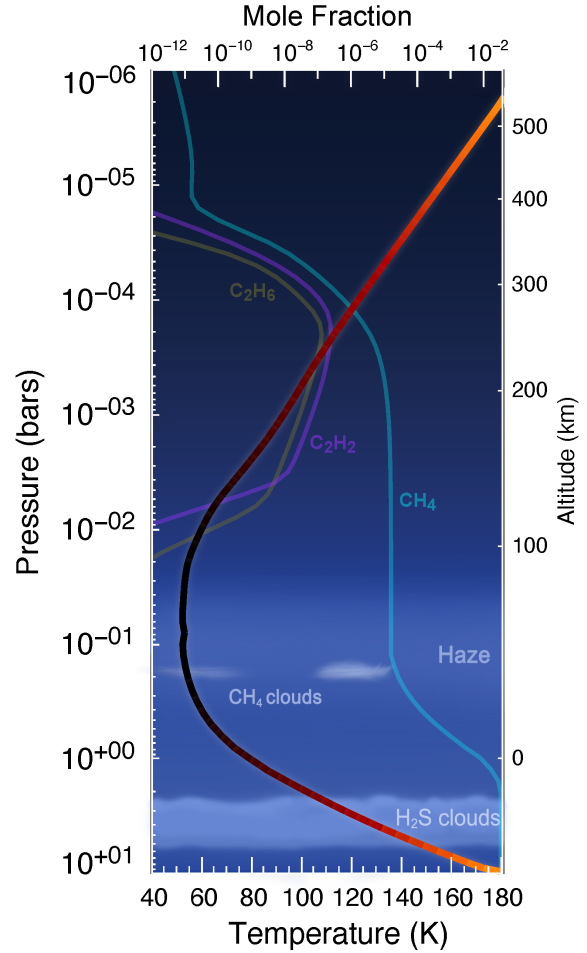


**Figure 4.** Uranus' temperature structure derived from Spitzer observations (Orton et al. 2014a), compared to the vertical profiles of methane, ethane, and acetylene (Moses et al. 2018) and the approximate locations of Uranus' CH<sub>4</sub> and H<sub>2</sub>S clouds. Credit: M.T. Roman.

radio occultations (Lindal et al. 1987). Cloud sounding via visible and near-IR spectroscopy (Fig. 3a) confirms the presence of optically-thin hazes in the upper troposphere and stratosphere, above a thin methane ice cloud near 1.3 bars, and thicker H<sub>2</sub>S cloud in the 2-4 bar range (Irwin et al. 2009; Tice et al. 2013; de Kleer et al. 2015).

H<sub>2</sub> and He become more enriched with height as the volatile gases condense out to form clouds, such that the observable upper troposphere is more 'dilute' and lacks signatures of H<sub>2</sub>O and NH<sub>3</sub> and is unlikely to be representative of the bulk. The helium mass fraction  $Y = 0.262 \pm 0.048$  was reported by Conrath et al. (1987) using Voyager data, which is just slightly less than the protosolar value (0.278) (Lodders et al. 2009).

The methane deep volume mixing ratios of (Sromovsky et al. 2019) suggest a bulk carbon enrichment

of  $\sim 50 - 85\times$  the protosolar abundance (Asplund et al. 2009), which is some ten times larger than that seen on the Gas Giants. However, there remains the possibility that the elements are not uniformly enriched. Radio observations (Gulkis et al. 1978; de Pater 1991) suggest a significant superabundance of  $\text{H}_2\text{S}$  ( $37_{-6}^{+13}\times$  protosolar) compared to  $\text{NH}_3$  ( $1.4_{-0.3}^{+0.5}\times$  solar) (Molter et al. 2021), which is quite different to Jupiter’s approximately solar N/S ratio, and the low abundance of sulphur in a solar-composition mixture. We expect  $\text{NH}_3$  and  $\text{H}_2\text{S}$  to combine to form a solid  $\text{NH}_4\text{SH}$  cloud layer in the 30-50 bar region (Weidenschilling and Lewis 1973; Sánchez-Lavega et al. 2004; Atreya and Wong 2005), leaving only the most abundant species -  $\text{H}_2\text{S}$  - at lower pressures (Deboer and Steffes 1994), as shown in Fig. 5. The superabundance of  $\text{H}_2\text{S}$  has been supported by measurements of microwave opacity of  $\text{H}_2\text{S}$  in the lab (DeBoer and Steffes 1996), and by the direct detection of  $\text{H}_2\text{S}$  vapour above the clouds in the H-band (Fig. 3a) near 1.57-1.58  $\mu\text{m}$  (Irwin et al. 2018). Condensation of  $\text{H}_2\text{S}$  ice therefore forms an important cloud deck near 2-4 bars. But does this sulphur excess imply a formation scenario where  $\text{H}_2\text{S}$  accretion was more efficient, potentially via trapping in clathrates (Hersant et al. 2004), or are we being misled because of chemistry in the deeper layers, where some  $\text{NH}_3$  and  $\text{H}_2\text{S}$  will be dissolved in a deep water (solution) cloud, a liquid water ocean at tens of kilobars, and potentially an ionic/superionic ocean and hundreds of kilobars (Atreya et al. 2020)? Even sampling the well-mixed abundances of  $\text{NH}_3$  and  $\text{H}_2\text{S}$  below the  $\text{NH}_4\text{SH}$  cloud will be challenging, given that  $\text{NH}_3$  is not well-mixed beneath the foreseen cloud base on Jupiter (Bolton et al. 2017).

Observationally, we find ourselves using tropospheric measurements in the  $\text{CH}_4$  ( $\sim 1.3$  bar) and  $\text{H}_2\text{S}$  (2-4 bar) cloud regions to infer the properties of Uranus’ deeper interior. The upper troposphere is effectively desiccated of other volatiles, so accessing Uranus’ bulk water abundance, and thus the O/H ratio, remains a significant challenge. Both planetary interior models (Guillot 1995) and measurements of CO (Cavalié et al. 2017; Venot et al. 2020) suggest that the  $\text{H}_2\text{O}$  abundance is potentially much larger, placing the water cloud base at hundreds of bars in Fig. 5. Not only is this inaccessible to an entry probe, but it is also a challenge for microwave sounding due to our lack of knowledge of the deep temperature structure, as measured thermal profiles from Voyager end at 2.3 bar (Lindal et al. 1987). Indeed, the potentially water-rich layers would cause lapse rates to depart substantially from adiabatic behaviour (Leconte et al. 2017), lending further complexity to Uranus’ deep temperature profile assumed in Fig. 5.

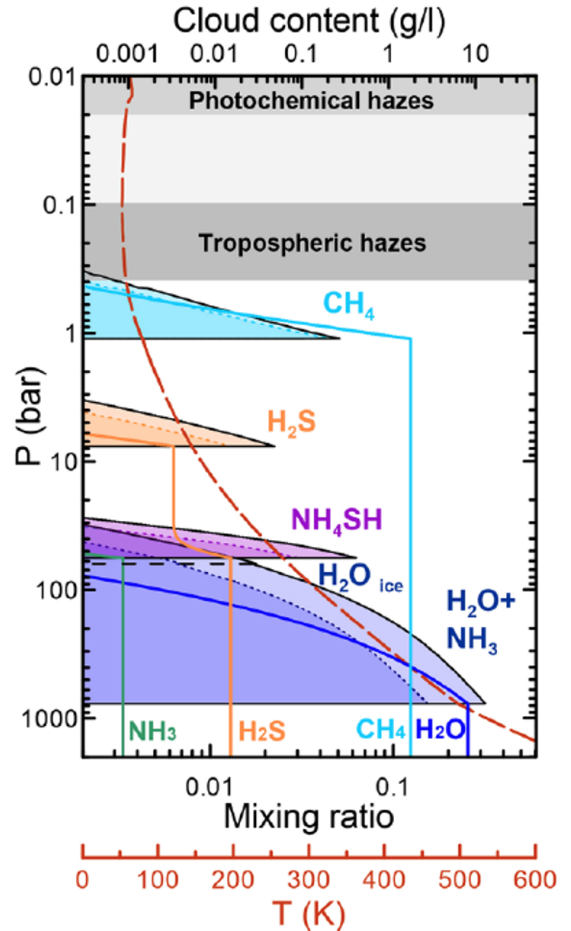


**Figure 5.** Approximate locations of Uranus’ clouds from thermochemical equilibrium condensation (Hueso and Sánchez-Lavega 2019). Mixing ratios of volatiles (lower axis) are for a  $30\times$  solar enrichment (approximately consistent with the  $37_{-6}^{+13}$  enrichment reported by Molter et al. 2021), except for  $\text{NH}_3$  which is assumed to be depleted ( $3\times$  solar). A moist adiabatic temperature profile, extrapolated from Voyager radio occultation profiles, is shown as the dashed red-brown line. Cloud densities (black continuous lines) are referenced to the top axis - see Fig. 9 of Hueso and Sánchez-Lavega (2019) for full details.

Estimating Uranus’ water content therefore relies on indirect approaches, such as using the chemistry of disequilibrium species. Thermochemical equilibrium controls composition in the deeper atmosphere (Fegley and Prinn 1986), but when the rate of vertical transport is faster than the rate of chemical destruction, the composition can be frozen in at abundances representative of the ‘quench’ point. Thus disequilibrium species can be studied at higher, colder altitudes, but none of the potential species studied by Fegley and Prinn (1986) have been definitively detected. CO, which is present in the stratosphere from external sources (Cavalié et al. 2013),

has only an upper limit in the troposphere (Teanby and Irwin 2013), so (Teanby et al. 2020) point out that there is no need to bring CO upwards from an oxygen-rich interior to explain the measurements. Nevertheless, if CO is present, then Cavalié et al. (2017) estimated that O/H is  $< 160\times$  the solar value in Uranus, but these have been revised downwards to  $< 45\times$  solar (Cavalié et al. 2020) using a revised chemical and transport scheme (Venot et al. 2020), highlighting the potential model-dependency associated with this approach. Vertical transport, parameterised through an eddy diffusion coefficient in these chemical schemes, may also depend on latitude, further confusing the picture. Ethane (Fegley and Lodders 1994) and  $\text{PH}_3$  could also be used to constrain O/H, but neither have been detected, and only upper limits are available for  $\text{PH}_3$  from millimetre wavelengths (Moreno et al. 2009; Teanby et al. 2019). And just as CO could aid in measuring the O/H abundance; molecular  $\text{N}_2$  could aid in the deep N/H abundance:  $\text{N}_2$  contributes to the molecular weight and collision-induced continua in the infrared, and while this has been studied on Neptune (Conrath et al. 1993), it has not been assessed on Uranus, in part because of the expected weak vertical mixing. Uranus’ bulk O/H, N/H and C/O ratios therefore remain extremely uncertain.

Further insights into the bulk composition come from isotopic ratios. The supersolar D/H ratio in  $\text{H}_2$  derived from Herschel measurements (Feuchtgruber et al. 2013) suggests accretion of a substantial water-ice-rich component, perhaps in addition to CO-rich ices (Ali-Dib et al. 2014) and rocky materials. Furthermore, if Uranus accreted from amorphous ices then each element (C, N, S, and the noble gases Ar, Kr, Xe) should show similar enrichments with respect to protosolar, as the trapping efficiencies in amorphous ices are similar at low temperatures (Owen et al. 1999). Alternatively, if the volatiles were originally trapped in clathrates, then the trapping efficiency can vary substantially from molecule to molecule (Mousis et al. 2018). Direct or indirect measurements of the elemental abundances in Uranus’ atmosphere are therefore needed to understand which primordial icy and rocky reservoirs contributed to Uranus during its formation (Mousis et al. 2018).

Having discussed the basic composition and vertical structure of Uranus’ atmosphere, Section 3 explores the various physical and chemical processes that reshape the temperatures, winds, clouds, and composition as a function of time and location.

### 3. ATMOSPHERIC PROCESSES

#### 3.1. Atmospheric Circulation

##### 3.1.1. Planetary Banding

The zonal, meridional, and vertical motions of Uranus’ troposphere and stratosphere may be studied via observations of zonal winds, temperature, composition, and aerosols, and how these parameters change over time. Contrast-enhanced images in reflected sunlight, such as those in Fig. 1-2 (Fry et al. 2012; Karkoschka 2015; Sromovsky et al. 2015) reveal a banded atmosphere, with fine-scale  $5-20^\circ$  latitudinal lanes of different reflectivity. These contrasts are probably due to variations in aerosol optical depth with latitude, although Karkoschka (2015) suggest that at least one of the bands could have been caused by variations in aerosol absorption, suggestive of different materials in some bands. Unlike Jupiter and Saturn, this banding appears to have no strong correlation with the zonal winds and temperatures (see Section 3.1.2), which means that we cannot define canonical Ice Giant ‘belts’ and ‘zones’ in quite the same way (Fletcher et al. 2020a). Furthermore, zonal medians of the reflectivity maps (Sromovsky et al. 2015) indicate that these zonal contrasts are not static, but change from observation to observation, potentially due to obscuration of the banded structure by discrete features. However, millimetre (1.3-3.1 mm) observations of Uranus from ALMA in 2017-2018, and centimetre (0.9-10 cm) observations from VLA in 2015 (Fig. 2, Molter et al. 2021) suggest subtle thermal banding in the 1-50 bar range that is qualitatively similar to that observed in reflected sunlight in the 1-4 bar range. This suggests that Uranus’ albedo contrasts could be related to thermal and/or compositional contrasts in the troposphere, although the long-term stability and location of the zonal bands remains to be rigorously assessed.

##### 3.1.2. Winds and Temperatures

Tropospheric zonal winds are constrained by tracking of discrete cloud features by Voyager 2 (Smith et al. 1986; Karkoschka 2015), the Hubble Space Telescope (Karkoschka 1998; Hammel et al. 2001), and ground-based facilities like Keck and Gemini (Sromovsky and Fry 2005; Hammel et al. 2005a; Sromovsky et al. 2009, 2015). These sources were used to develop a ‘canonical wind profile’ by fitting Legendre polynomials to the measured drift of features (Fig. 6c, Sromovsky et al. 2015), although there remains some dispersion and potential temporal variations around these measurements. Most of the tracked cloud features on Uranus are near the 1.3-bar methane condensation level or in the deeper 2-4 bar main clouds of  $\text{H}_2\text{S}$  ice (Irwin et al. 2018), but some can reach the 250-600 mbar region in the upper troposphere (Sromovsky et al. 2007, 2012; Roman et al. 2018). Some of the smaller-scale clouds evolve quite rapidly (Irwin et al. 2017), making it difficult to track them over multi-

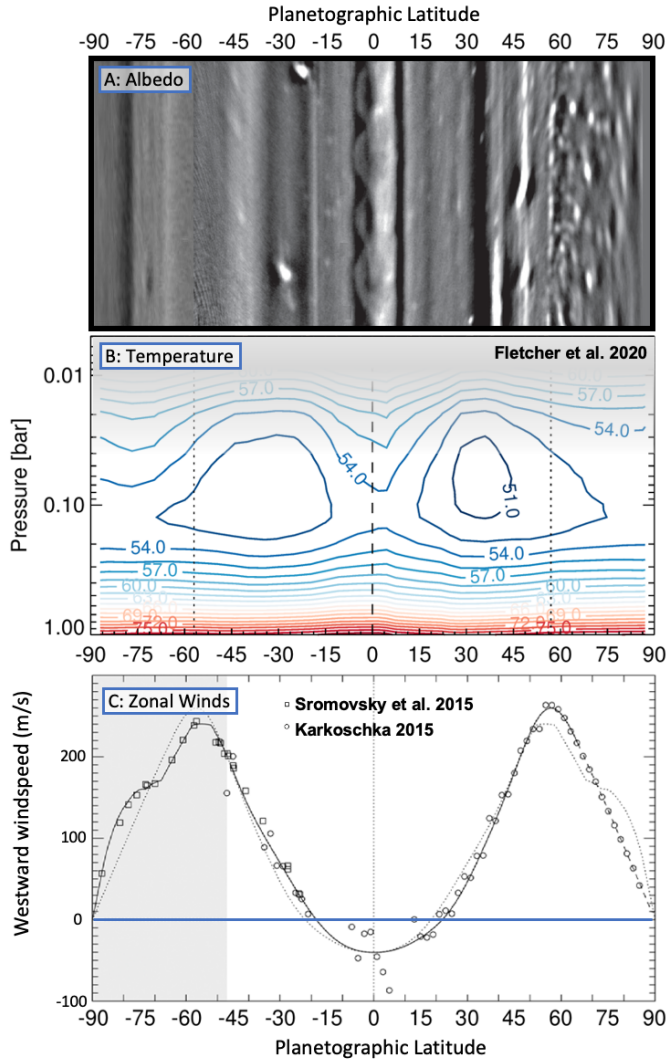


**Figure 6.** Comparison of Uranus’ near-IR reflectivity (A) to the zonal-mean tropospheric temperatures (B) and cloud-tracked winds (C). In panel (A) we show Voyager-2 imagery poleward of  $60^{\circ}\text{S}$  (Karkoschka 2015) with Keck H-band imagery in 2012 northward of  $60^{\circ}\text{S}$  (Sromovsky et al. 2015). Panel (B) comes from inversion of Voyager/IRIS 25–50  $\mu\text{m}$  spectroscopy (Fletcher et al. 2020a), the grey shaded regions represent the declining information content at low pressures. Zonal winds in (C) are adapted from Fig. 15 of Sromovsky et al. (2015), combining Voyager-2 observations in the grey shaded area (squares, Karkoschka 2015) with Keck observations (circles) at other latitudes, and the dotted curve represents a profile if reflected at the equator.

ple rotations. Nevertheless, Fig. 6 shows that the cloud tracking has revealed a single, broad retrograde jet at Uranus’ equator, and a single high-latitude  $\sim 260$  m/s prograde jet in each hemisphere near  $50\text{--}60^{\circ}$ , quite unlike the multi-jet circulations of Jupiter and Saturn (see the reviews by Sanchez-Lavega et al. 2019). Note that it

is common practice to define Uranus’ westward winds as positive (prograde), and the eastward equatorial jet as negative (retrograde), unlike on the other giants. Furthermore, reconstruction of the gravity field measured by Voyager 2 (Hubbard et al. 1991) out to the fourth order harmonic (Kaspi et al. 2013) suggests that these tropospheric winds are confined to a layer approximately 1000 km deep (i.e., down to 2 kbar).

Geostrophic balance suggests that we should measure a correlation between horizontal temperature gradients and the vertical shear on the zonal winds (Holton 2004). The thermal banding observed in the microwave in Fig. 2 (Molter et al. 2021) is too fine-scale to be related to the broad structure of the zonal flow (Sromovsky et al. 2015), but thermal-IR observations by Voyager 2 (Flasar et al. 1987; Conrath et al. 1998) and ground-based facilities (Fig. 2, Orton et al. 2015; Roman et al. 2020) reveal larger-scale structure, with cool mid-latitudes in the 80–800 mbar range, contrasted with a warmer equator and poles. The tropospheric temperature patterns in Fig. 6b appear to be unchanging in the time since Voyager 2, and imply maximum positive windshears near  $\pm(15\text{--}30)^{\circ}$  latitude on the flanks of the equatorial retrograde jet, and maximum negative windshear near the high-latitude prograde jets at  $\pm(60\text{--}75)^{\circ}$  (Fletcher et al. 2020a). The windshear is minimal (i.e., close to barotropic, with no wind variability with height) in the  $\pm 30\text{--}50^{\circ}$  latitude range associated with the mid-latitude temperature minima, which is also where the most notable storm activity occurs (Section 3.2). Taken together, this suggests that the cloud-top prograde jets of Sromovsky et al. (2015) should decay with altitude, potentially due to frictional damping related to the breaking of vertically propagating waves in the upper troposphere (Flasar et al. 1987). The equatorial winds would be more complicated, with the most rapid decay of the retrograde flow with height occurring away from the equator. Furthermore, existing measurements of latitudinal temperature gradients and zonal winds have relatively poor spatial resolution, so it is reasonable to assume that finer-scale temperature/wind bands exist throughout the troposphere, as suggested by the reflectivity (Fig. 6a) and microwave emission maps. Future missions with multi-spectral mapping capabilities are needed to resolve this.

Finally, there are hints in Fig. 6 that both the zonal winds (Sromovsky et al. 2015) and the tropospheric temperatures (Conrath et al. 1998; Orton et al. 2015) exhibit a north-south asymmetry, and that this asymmetry might be weakening with time. Southern summertime winds at  $50\text{--}90^{\circ}\text{S}$  (Karkoschka 2015) appear to be very different to corresponding northern latitudes  $60\text{--}83^{\circ}\text{N}$



during spring (Sromovsky et al. 2015), where zonal drift rates adhere to solid-body rotation. Long-term tracking of the winds will be required to understand whether this asymmetry is seasonal, or a permanent feature.

### 3.1.3. Composition Contrasts

Besides temperatures, winds, and aerosols, we also observe planetary banding in the gaseous composition in Fig. 7. Fine-scale banding in microwave emission in Fig. 7c (Molter et al. 2021) has already been discussed, and can be interpreted in terms of variations in  $\text{H}_2\text{S}$  abundance as a function of latitude. The collision-induced continuum measured by Voyager 2 also reveals the latitudinal contrasts in para-hydrogen, the even spin isomer of  $\text{H}_2$  (Flasar et al. 1987; Conrath et al. 1998; Fletcher et al. 2020a). The para- $\text{H}_2$  fraction is quenched at 25% in the warmer deep troposphere, and chemical equilibration is sufficiently slow that upward motion can bring this low-para- $\text{H}_2$  air upwards into the cooler upper troposphere, where the equilibrium para- $\text{H}_2$  abundance should be much larger. Sub-equilibrium para- $\text{H}_2$  in Fig. 7a is therefore indicative of upwelling, which is seen at mid-latitudes in the 80-800 mbar region. Conversely, super-equilibrium para- $\text{H}_2$  is observed at the equator and poles, which is taken to be an indicator of subsidence from the cold tropopause. Caution is required though, as poorly-understood catalysis processes on aerosol surfaces could cause the equilibration timescale to vary with location (Massie and Hunten 1982).

Small-scale contrasts in Fig. 7b-c are superimposed onto a significant equator-to-pole decline in the volatile abundances  $\text{CH}_4$  and  $\text{H}_2\text{S}$ . Uranus' south polar depletion of methane was first detected via Hubble 300-1000 nm spectroscopy in 2002 (Karkoschka and Tomasko 2009), when the north polar region was still largely hidden from view. After equinox in 2007, further Hubble observations in 2012 (Sromovsky et al. 2014) and 2015 (Sromovsky et al. 2019) revealed that the north polar region exhibited a similar depletion, and that the equator-to-pole gradient from  $\sim 4\%$  near the equator to  $\sim 2\%$  at high latitudes appeared to be relatively stable over time. Furthermore, this gradient exhibited a step-like structure, with a transition in abundance near the  $\pm 30 - 40^\circ$  latitude region, although degeneracies with the assumed aerosol distribution can modify the derived gradients. Uranus' polar methane depletion was also observed independently from ground-based facilities in the near-infrared, including the IRTF (Tice et al. 2013), Keck (de Kleer et al. 2015), Palomar (Roman et al. 2018), the VLT and Gemini (Toledo et al. 2018; Irwin et al. 2018). Sromovsky et al. (2019) reproduced the spectra with a methane distribution that was latitudinally uniform for

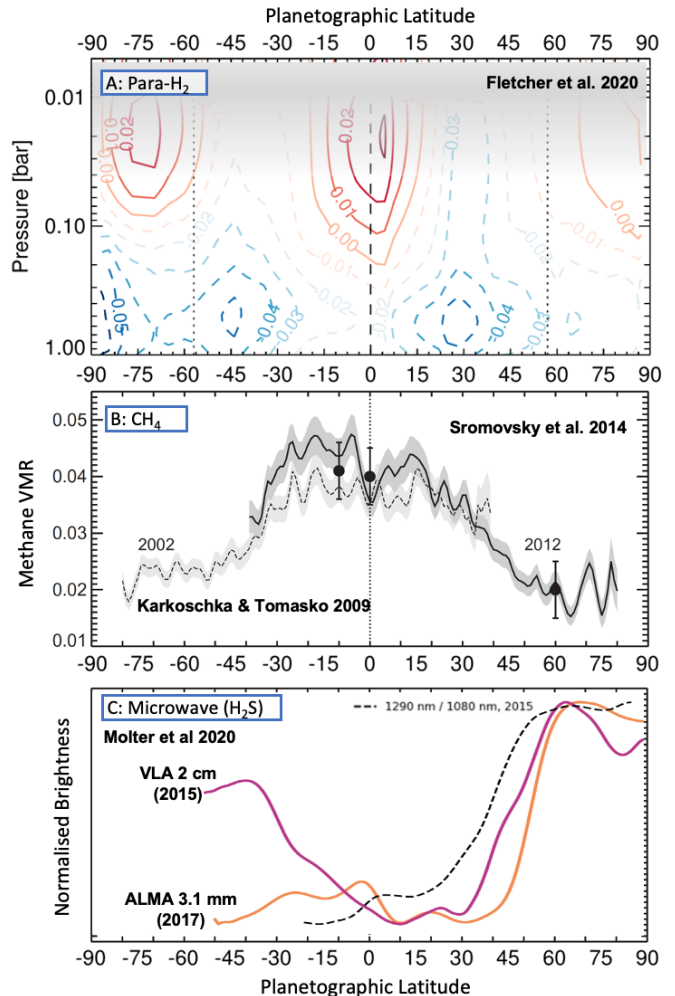


**Figure 7.** Zonal-mean composition gradients in para- $\text{H}_2$  disequilibrium (A), tropospheric  $\text{CH}_4$  (B), and tropospheric microwave emission indicating  $\text{H}_2\text{S}$  variations (C). Panel (A) shows the extent of disequilibrium for para- $\text{H}_2$  (sub-equilibrium in dotted lines indicating upwelling, super-equilibrium in solid lines indicating subsidence) derived from Voyager/IRIS spectra (Fletcher et al. 2020a). Grey shading indicates the lack of information content for  $p < 70$  mbar. The latitudinal distribution of methane in panel (B) is from Karkoschka and Tomasko (2009); Sromovsky et al. (2014). The deep distribution of  $\text{H}_2\text{S}$  is represented by the normalised microwave brightness in panel (C), as measured by ALMA and the VLA (Molter et al. 2021), where higher emission indicated depleted  $\text{H}_2\text{S}$  abundances, and the dashed line is indicative of the poleward  $\text{CH}_4$  depletion as given in panel (B).

$p > 5$  bar (in the 2.7-3.5% range, depending on aerosol scattering properties), and only latitudinally variable at lower pressures in the upper troposphere, with a factor of three decrease in the upper tropospheric  $\text{CH}_4$  from  $30^\circ\text{N}$  to  $70^\circ\text{N}$ .

However, the implied equator-to-pole circulation, with rising methane-rich air at low latitudes, moving polewards as  $\text{CH}_4$  is removed by condensation, precipitation, and sedimentation, before methane-poor air sinks at high latitudes, may in fact extend much deeper. VLA centimetre observations of Uranus between 1982 and 1994 (de Pater and Gulkis 1988; de Pater 1991; Hofstadter and Butler 2003), probing down to 50 bar, revealed Uranus’ microwave-bright south polar region due to a strong depletion absorbers, with a strong brightness gradient near  $45^\circ\text{S}$  (Fig. 2). VLA observations since 2003 show that the north polar region was similarly bright (Hofstadter et al. 2004; de Pater et al. 2018; Molter et al. 2021), and this high brightness can be primarily explained by the absence of  $\text{H}_2\text{S}$  down to  $\sim 35$  bars (Molter et al. 2021). Whether this polar depletion of deep  $\text{H}_2\text{S}$  is caused by the same circulation and subsidence responsible for the shallow  $\text{CH}_4$  depletion is an open question (Sromovsky et al. 2014; Fletcher et al. 2020a). Furthermore, neither the methane nor the  $\text{H}_2\text{S}$  appear to be tracing the upper tropospheric circulation revealed by the para- $\text{H}_2$  and temperature distribution, which would suggest mid-latitude upwelling, rather than equatorial upwelling. Indeed, polar subsidence would tend to inhibit convection and  $\text{CH}_4$  cloud formation (Sromovsky et al. 2012), and yet discrete clouds were clearly visible at Uranus’ north pole during early northern spring in Fig. 1 (Sromovsky et al. 2014).

### 3.1.4. Meridional Overturning

Uranus’ tropospheric circulation has yet to be explored via detailed numerical simulation, but the differences between (i) the broad contrasts in upper tropospheric temperatures, winds and para- $\text{H}_2$ ; (ii) the fine-scale banding observed in the aerosols and deep thermal emission; and (iii) the strong equator-to-pole contrasts in  $\text{CH}_4$  and  $\text{H}_2\text{S}$ , imply that circulation cells might be restricted to two or more discrete tropospheric layers (Sromovsky et al. 2015; Fletcher et al. 2020a). Similar ‘stacked circulation cells’ have been proposed for Jupiter and Saturn (Ingersoll et al. 2000; Showman and de Pater 2005; Fletcher et al. 2020c), and it is possible that the stabilising influence of molecular weight gradients where clouds condense might help in separating these layers, creating stable regions where convection is inhibited (Guillot 1995; Leconte et al. 2017; Friedson and Gonzales 2017), and possibly preventing vertically-extended convection and circulation entirely. Indeed, thin-layered convection was proposed to explain Voyager observations of Uranus’ lapse rate and para- $\text{H}_2$  distribution by (Gierasch and Conrath 1987). The  $\text{CH}_4$  and  $\text{H}_2\text{S}$  condensation levels may be good candidates for

transitional layers, decoupling motions above and below (Hueso and Sánchez-Lavega 2019). Such differences in atmospheric circulation as a function of depth remain to be proven, but the transition from a deep domain where eddies provide momentum to the zonal jets, to a shallow domain where zonal jets decay with altitude due to unidentified frictional drag (i.e., a radiative- or wave-driven circulation regime), remains a plausible explanation for the multi-spectral observations available today.

Finally, we note that the tropospheric circulation may also have implications for Uranus’ stratosphere. Stratospheric chemistry will be discussed in Section 3.3, but we note that photolysis of stratospheric methane produces acetylene,  $\text{C}_2\text{H}_2$ , which is the only stratospheric chemical to have been mapped on Uranus to date (Roman et al. 2020). Using images at  $13.7 \mu\text{m}$ , Roman et al. (2020) revealed excess  $\text{C}_2\text{H}_2$  emission at mid-latitudes, counter to the expectations of seasonal photochemical models (Moses et al. 2018). They proposed two equally plausible mechanisms: either tropospheric mid-latitude upwelling was transporting methane-rich air through the cold trap and into the stratosphere, where it was subsequently photolysed to form  $\text{C}_2\text{H}_2$ ; or the stratosphere exhibited subsidence and adiabatic warming at mid-latitudes. The first case can be considered as an upward extension of the upper tropospheric circulation, whereas the second case is a circulation where the mid-latitude stratospheric subsidence opposes the mid-latitude tropospheric upwelling, yet another tier of a stacked circulation system. Distinguishing between these two possibilities is a topic of ongoing research.

## 3.2. Uranian Meteorology

### 3.2.1. Convective Storms

Discrete meteorological features, from small bright clouds, to planet-encircling waves, giant storms and dark vortices, are superimposed upon and intricately connected to the large-scale atmospheric circulation described in Section 3.1. Some of the small-scale bright clouds, presumably comprised of methane ice reaching pressures of 300-600 mbar, high above the main  $\text{H}_2\text{S}$  cloud deck at 2-4 bars, may be convective in origin, driven by a combination of latent heat release as  $\text{CH}_4$  condenses (Stoker and Toon 1989; Hueso et al. 2020), and potentially by the energy released during the interconversion between para- and ortho- $\text{H}_2$ , which have different specific heats (Smith and Gierasch 1995). However, Uranus shares the same problem as the other giant planets, in that air saturated with condensates will be heavier than the surrounding ‘dry’  $\text{H}_2$ -He mixture (Guillot 1995; Leconte et al. 2017; Friedson and Gonza-

les 2017). As described in Section 3.1, the strong vertical gradient in molecular weight prevents convection extending over tremendous heights, instead limiting it to vertically-thin layers (Gierasch and Conrath 1987). Strong initial perturbations are therefore required to counteract this static stability (effectively a negative buoyancy) to drive self-sustaining CH<sub>4</sub>-rich updrafts, but this has yet to be verified observationally (Hueso and Sánchez-Lavega 2019; Hueso et al. 2020). Indeed, Guillot (2019) point out that this moist CH<sub>4</sub>-driven convection is occurring at shallow pressures (0.1-1.5 bars) and low optical depths compared to the deep, hidden H<sub>2</sub>O clouds of Jupiter and Saturn, meaning that Uranus (and Neptune) provide ideal destinations to investigate how convection operates on hydrogen-rich worlds where it is inhibited by the weight of the condensables. Furthermore, Uranus’ moist convection might be rather different to Jupiter’s, as H<sub>2</sub>O will play a very limited role in the observable upper troposphere, and H<sub>2</sub>S condensation provides only a limited source of latent heat to drive convection.

Hueso et al. (2020) define Uranus’ convective features to be storm features that show divergence above the clouds over short timescales, but they point out that the frequency and distribution of such storms is not well known, and much of the observed cloud activity might not be convective. Instead, some bright features may be orographic structures associated with pressure perturbations at deeper levels (e.g., those associated with dark, hidden vortices), which do not require buoyancy to produce condensation, as on Neptune (Stratman et al. 2001). A particularly long-lived feature at southern mid-latitudes, some 5000-10000 km wide, was known as the ‘Berg’ and had bright features rising to the 550-750 mbar level, but with the main parts of the structure near 1.7-3.5 bars (de Pater et al. 2011). The berg was captured by HST and Keck between 1994 and 2009 (Sromovsky et al. 2009; de Pater et al. 2011; Hammel et al. 2005a; de Pater et al. 2015; Sromovsky et al. 2015), and may even have been observed by Voyager in 1986 (Sromovsky and Fry 2005). It oscillated in latitude (around 35.2°S) and longitude, migrating towards the equator after 2005, reaching 27°S in 2007, and disintegrating when it reached 5°S in late 2009 (Sromovsky et al. 2009; de Pater et al. 2011). The Berg exhibited intense brightenings in 2004 and 2007 suggestive of convective storms within the feature (de Pater et al. 2015), but there was no evidence that it was related to a deeper unobserved vortex (Hueso and Sánchez-Lavega 2019).

Discussion of strong convection naturally raises questions about the potential for lightning. Methane is non-polar, but H<sub>2</sub>S, NH<sub>3</sub>, NH<sub>4</sub>SH and H<sub>2</sub>O provide

the mixed-phase materials that could produce lightning (Aplin et al. 2020). Microphysical modelling suggesting that the radio emissions discovered by Voyager (Zarka and Pedersen 1986) are more likely related to the NH<sub>4</sub>SH cloud than the deep water layers (Aplin et al. 2020).

### 3.2.2. Discrete Cloud Activity

Uranus has exhibited a range of discrete cloud phenomena since the early Voyager and Hubble observations. Eight features were observed between 35 – 70°S by Voyager (Smith et al. 1986) near northern winter solstice. As winter proceeded in the mid-1990s, notable bright cloud features were observed at mid northern latitudes (Karkoschka 1998), as they were emerging into sunlight. Since 2000, ground-based facilities like Keck were frequently detecting cloud features (Hammel et al. 2001; de Pater et al. 2002; Hammel et al. 2005a), including some in 2004 that reached sufficiently high altitude to be detected in the strong CH<sub>4</sub> band near 2.12 μm (Hammel et al. 2005b). Northern mid-latitudes 28 – 42°N appear to be intrinsically active (Sromovsky and Fry 2007), particularly in the years following northern spring equinox ( $L_s = 0^\circ$ , 2007), with clouds reaching 300-500 mbar, and new outbreaks observed in 2004-06 and 2011 (Sromovsky et al. 2007, 2009, 2012). A record-breaking bright storm occurred at 15°N in 2014, as shown in Fig. 2 (de Pater et al. 2015), thought to be formed from a complex of smaller storms. And another at 32°N possessed a longitudinally-elongated tail in the 1-2 bar range, qualitatively similar to storm tails observed on Jupiter and Saturn (de Pater et al. 2015; Sromovsky et al. 2015; Irwin et al. 2016, 2017).

It is natural to ask whether Uranian storms exhibit a temporal dependency, given that some of the brightest activity appeared to occur in the hemisphere emerging from the darkness of winter. Alternatively, maybe Uranian storms occur episodically due to powerful outbursts followed by long periods of quiescence as CAPE (convective available potential energy) accumulates, as suggested for Saturn’s annual storms (Li and Ingersoll 2015). However, storm statistics are currently insufficient, and the observations are biased to the sunlit hemisphere, so robust assessment of the destabilising influence of increased insolation remains to be performed. The one exception is in the polar domain in Fig. 1, where the south pole displayed no discrete activity during southern summer (Smith et al. 1986; Karkoschka 2015), whereas clusters of bright spots with 600-800 km diameters were observed in the north polar region after it emerged into sunlight in northern spring (Sromovsky et al. 2012, 2015). This notable asymmetry suggests

some form of convective inhibition (or obscuration by overlying hazes) developing as spring turns to summer, something which will be testable as Uranus approaches northern summer solstice ( $L_s = 90^\circ$ ) in 2030.

### 3.2.3. Vortices and Waves

The vast majority of discrete features tracked on Uranus have been bright cloud features, rising above the main cloud decks. However, Uranus also infrequently exhibits dark anticyclonic ovals, which can form and dissipate on the timescales of years. Hubble was the first to observe a dark vortex in 2006 at  $28^\circ\text{N}$  (Hammel et al. 2009), and since that time several more have been observed (e.g., Sromovsky et al. 2015). These are typically smaller than those observed on Neptune, and whether they are accompanied by bright (and more readily visible) companion clouds due to air being forced up and over the vortex (orographic clouds, Stratman et al. 2001) remains a topic of ongoing exploration. It is not clear whether the dearth of anticyclonic ovals on Uranus with respect to Neptune is an observational bias (e.g., due to different overlying aerosols and gas absorption), or a real difference between the two worlds.

Finally, Uranus exhibits wave phenomena that manifest as longitudinal reflectivity contrasts in the troposphere. A chain of diffuse bright features just north of the equator, first suggested by Keck images in 2003 (Hammel et al. 2005a), were observed by Keck in 2012 (Sromovsky et al. 2015) to be spaced every  $30 - 40^\circ$  longitude. A second wave was captured by the 2012-14 Keck observations using adaptive optics and derotation techniques (Fig. 6a, Fry et al. 2012; Sromovsky et al. 2015), revealing a transverse ‘scaloped’ equatorial wave pattern, just south of the equator, with diffuse bright features every  $19 - 21^\circ$  longitude (wavenumber 17-19) and a latitudinal amplitude of  $2.4 - 2.9^\circ$ . Sromovsky et al. (2015) suggest that Kelvin waves or mixed internal gravity-Rossby waves may be at work, but that this cannot be properly characterised until the dispersion relation (phase speed versus wavelength) is determined.

Wave phenomena are unlikely to be restricted to Uranus’ troposphere, and may also be present in the stratosphere, modulating emission from stratospheric hydrocarbons (Roman et al. 2020) and generating rotational variability in disc-averaged mid-IR spectra observed by Spitzer (Rowe-Gurney et al. 2021).

## 3.3. Chemistry

Although the thermochemistry and condensation chemistry of Uranus’s troposphere were described in Section 2, the influence of UV photolysis, coupled with the atmospheric circulation (Section 3.1), can contribute to the sources, sinks, and spatio-temporal distributions of

chemicals detected in Uranus’ upper troposphere and stratosphere. Whilst much of this section will be devoted to stratospheric chemistry, photolysis of the yet-to-be detected  $\text{PH}_3$  (Moreno et al. 2009; Teanby et al. 2019) and  $\text{H}_2\text{S}$  lofted to high altitude may contribute to upper tropospheric hazes, and potentially more so than on Jupiter and Saturn because of the absence of  $\text{NH}_3$  to act as a UV shield (Visscher and Fegley 2005; Moses et al. 2020).

### 3.3.1. Methane Photochemistry

Methane photolysis products dominate the stratospheric composition of both Ice Giants (Atreya et al. 1991), but the strength of vertical mixing by eddy diffusion (weak on Uranus, strong on Neptune) has stark consequences for the distribution of species, with Uranian methane photochemistry operating in a higher-pressure regime than on any other giant planet (Moses et al. 2018). The lower  $\text{CH}_4$  homopause on Uranus (Herbert et al. 1987) has the surprising consequence that seasonal contrasts are more muted than on Neptune, and that  $\text{CH}_4$  chemistry is not as well coupled to exogenic oxygenated materials deposited at lower pressures (see Section 3.3.2). Nevertheless, photochemistry on Uranus results in a complicated mix of hydrocarbons (Atreya and Ponthieu 1983; Moses et al. 2005; Dobrijevic et al. 2010; Moses et al. 2018) that can be investigated via mid-infrared remote sensing (Orton et al. 1987; Feuchtgruber et al. 1997; Encrenaz et al. 1998; Orton et al. 2014a; Roman et al. 2020; Rowe-Gurney et al. 2021) and UV occultations (Herbert et al. 1987; Bishop et al. 1990). Acetylene ( $\text{C}_2\text{H}_2$ ) was first discovered by ISO (Encrenaz et al. 1998); ethane ( $\text{C}_2\text{H}_6$ ), methyl-acetylene ( $\text{C}_3\text{H}_4$ ) and diacetylene ( $\text{C}_4\text{H}_2$ ) were observed by Spitzer (Burgdorf et al. 2006; Orton et al. 2014b). Some products, such as ethylene, propane, benzene and methyl have not yet been detected (Moses et al. 2020). The effects of the high-pressure photochemistry are apparent in mid-IR observations: Uranus’ hydrocarbons are confined to altitudes below the  $\sim 0.1$ -mbar level in Fig. 4, and the ratio of ethane to acetylene is very different on Uranus compared to all the other giants (Orton et al. 2014b).

The latitudinal distribution of these species is expected to vary due to stratospheric circulation and seasonal photochemistry (Fig. 8). Although photochemistry occurs primarily in UV sunlight (145 nm), and thus photolytic rates will be largest at polar latitudes that receive a higher annual-average solar insolation than the equator, small amounts of solar Lyman alpha scattered from hydrogen in the local ISM can provide a secondary photolysis source during the darkness of winter.



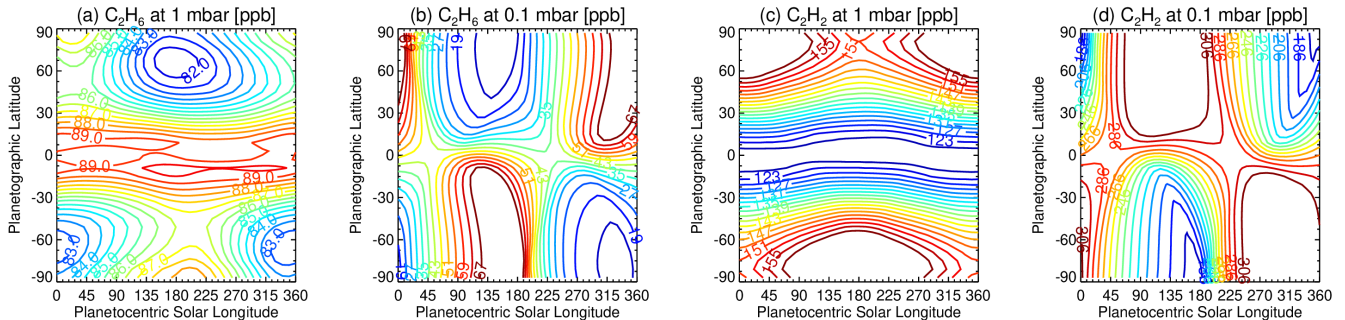


**Figure 8.** Predicted contrasts in abundances of stratospheric hydrocarbons ethane ( $C_2H_6$ ) and acetylene ( $C_2H_2$ ) at 0.1 and 1 mbar in parts per billion. Each panel shows the abundance as a function of latitude and planetocentric solar longitude, revealing larger variations at lower pressures, and the different behaviours of these two species. Plotted from the seasonal photochemistry model of Moses et al. (2018).

Chemical abundances respond quickly at low pressures to changes in the UV flux, but Fig. 8 shows that contrasts should decrease at higher pressures, where diffusion and chemical timescales increase, producing subtle hemispheric asymmetries at  $p < 1$  mbar with phase lags in response to insolation changes (Moses et al. 2018). Thus short-lived species like acetylene, methyl-acetylene and diacetylene are expected to have maximum abundances at the summer/autumn poles, whereas long-lived species like ethane are expected to peak near the equator because photolytic destruction effectively competes with production in the high-latitude summer. However, these predictions assume uniform distributions of stratospheric  $CH_4$  as the source material, which may not be the case given the strong equator-to-pole  $CH_4$  gradients in the troposphere (Section 3.1.3). Furthermore, there remains some disagreement about what the stratospheric  $CH_4$  abundance actually is, with a factor of six in stratospheric abundance between Spitzer results in 2007 (Orton et al. 2014b) and Herschel results in 2011 (Lellouch et al. 2015). Both inferences were from disc-integrated spectra, so this could be a sign of changing viewing geometry, latitudinal temperature gradients, changes in efficiency of vertical mixing, temporal variability, or some combination of the above.

Of these species, only emission from  $C_2H_2$  has been mapped across Uranus, showing stark discrepancies from the photochemical model predictions (Moses et al. 2018; Roman et al. 2020), and implying a key role for circulation: either strong mid-latitude upwelling of  $CH_4$ -rich air from the troposphere; or mid-latitude subsidence in the stratosphere (Section 3.1). The ground-based VLT maps of stratospheric  $C_2H_2$  emission in Fig. 2 suggest a distinct equatorial minimum at latitudes  $< \pm 25^\circ$  (Roman et al. 2020), counter to photochemical expectations and the complete opposite of what is observed in the tropospheric temperatures.

The products of  $CH_4$  photochemistry, such as benzene, acetylene, ethane and propane (in addition to exogenic  $H_2O$  and  $CO_2$ ) can condense to form thin haze layers in the 0.1-30 mbar range (Fig. 4 and 5), some of which are visible in high-phase imaging from Voyager (Rages et al. 1991; Romani et al. 1993; Moses and Poppe 2017; Toledo et al. 2018) and may be modulated by vertically propagating waves. The condensed hydrocarbons could also sediment downwards to coat tropospheric hazes, or serve as cloud-condensation nuclei for  $CH_4$  and  $H_2S$  condensation at higher pressures.

### 3.3.2. Coupling to External Oxygen

Oxygen species like  $CO$ ,  $CO_2$  and  $H_2O$  are present in the upper stratospheres of each of the giant planets (Feuchtgruber et al. 1997; Moses and Poppe 2017), originating from cometary impacts, satellite debris, and ablation of interplanetary dust and ring particles. What makes Uranian photochemistry particularly interesting is that this oxygen deposition is separated from the methane photochemistry due to the sluggish vertical mixing, making it an intriguing counterpoint to the other giants (Moses and Poppe 2017). Uranus' stratospheric water was detected by ISO (Feuchtgruber et al. 1997);  $CO$  from the fluorescent emission in the infrared (Encrenaz et al. 2004) and sub-millimeter emission (Cavalié et al. 2013); and  $CO_2$  from Spitzer (Burgdorf et al. 2006; Orton et al. 2014a). Photolysis of  $CO$  and  $CO_2$  can lead to secondary peaks of hydrocarbon production at high altitudes above the levels where the  $CH_4$  abundance is dropping away (Moses et al. 2018), whereas  $H_2O$  will condense to form a 10-mbar ice haze. An interplanetary dust particle source is sufficient to explain the observed amount of  $CO$ ,  $CO_2$  and  $H_2O$  in Uranus' stratosphere (Moses and Poppe 2017), although cometary impacts could also contribute (Lara et al. 2019).

### 3.3.3. Radiative Balance

The vertical distribution of hydrocarbons, particularly  $\text{CH}_4$ ,  $\text{C}_2\text{H}_2$  and  $\text{C}_2\text{H}_6$ , determine the radiative heating and cooling in Uranus' middle atmosphere. For this reason, the influence of thin hazes and secondary peaks of hydrocarbon production can have a significant influence. Uranus' upper troposphere and stratosphere is warmed by shortwave absorption by  $\text{CH}_4$  and aerosols, and cooled by longwave emission from  $\text{C}_2\text{H}_2$  and  $\text{C}_2\text{H}_6$  in the stratosphere, and from the collision-induced  $\text{H}_2$ -He continuum in the troposphere (Conrath et al. 1998; Li et al. 2018). However, it has long been noted that absorption of weak sunlight by  $\text{CH}_4$  alone cannot balance the efficient cooling from  $\text{H}_2$  and, to a lesser extent, the hydrocarbons, so the middle atmosphere is warmer (Orton et al. 2014a) than expected. Additional sources of heat from vertically propagating gravity waves or the radiative contribution of hazes have been invoked to explain the discrepancy between observations and predictions (Li et al. 2018).

Uranus' extreme obliquity, resulting in a larger irradiance at the poles than the equator, could also yield seasonal temperature asymmetries. However, Uranus' radiative time constant in the troposphere is longer than the Uranian year (Friedson and Ingersoll 1987; Conrath et al. 1990), such that tropospheric temperatures are not expected to change significantly with time, and to track the annual-average equilibrium values (Lunine 1993). This is consistent with the lack of observed tropospheric temperature variation between Voyager (Fig. 6) and the present day (Orton et al. 2015; Roman et al. 2020). Stratospheric temperature asymmetries have never been measured because of the extreme cold and resulting low mid-IR radiance, but we note that Uranus' stratospheric radiative time constant is actually longer than that on Neptune, due to the low  $\text{CH}_4$  abundance and cold temperatures, such that stratospheric temperature asymmetries might be weaker on Uranus and again simply track the annual average (i.e., warmer at the poles, and cooler at the equator). Future missions capable of measuring temperature contrasts between the summer and winter hemisphere are needed to address this question.

### 3.4. Temporal Change

A theme running through our discussion of Uranus' circulation (Section 3.1), meteorology (Section 3.2) and chemistry (Section 3.3), is that we can learn more about a system by observing how it evolves with time. Given that resolved observations of Uranus' atmosphere spans almost four decades, and photometric observations span even longer, Uranus is the ideal testbed for studying variability on an Ice Giant. We have already

described three time-variable aspects of Uranus' atmosphere. Firstly, predictions of radiative-climate models and diffusive photochemistry models suggest that upper tropospheric and stratospheric temperatures and hydrocarbon distributions might show subtle hemispheric asymmetries that reverse as seasons progress, but that the relevant time constants are so long that such contrasts are expected to be small. Nevertheless, subtle mid-latitude asymmetries in tropospheric temperatures (Conrath et al. 1998) and winds (Sromovsky et al. 2015) have been observed. Secondly, high-latitude winds were found to be different between northern spring in 2012-14 (where a broad region of solid-body rotation from 62-83°N was identified, Sromovsky et al. 2015) and southern summer in 1986 (with a much smaller region of solid-body rotation, Karkoschka 2015). Whether this is a permanent asymmetry, or something that will change as northern summer solstice approaches in 2030, remains to be seen. Thirdly, there is evidence that small-scale cloud and storm activity varies over time, potentially as a result of the changing atmospheric stability as the seasons change, and this is particularly notable in the polar domain (Sromovsky et al. 2012).

These three time-variable processes are dwarfed by long-term variations associated with Uranus' seasonal polar cap and collars (Fig. 9), which are likely related to the processes discussed above and which modulate the disc-integrated photometry as seen from Earth (Lockwood 2019). Voyager observations during southern summer revealed a reflective polar cap poleward of 45°S, originally thought to be due to an increase in the optical depth of the  $\text{CH}_4$  clouds near 1.2-1.3 bars (Rages et al. 1991). In the years after Voyager, Hubble observations between 1994 and 2002 revealed a darkening of the south pole (Fig. 9), the formation of a bright ring near 70°S and a south polar collar at 45°S (Rages et al. 2004). As the northern hemisphere came into view after 2007, the south polar collar diminished (Irwin et al. 2010; Roman et al. 2018), and a north polar collar developed at 45°N (Irwin et al. 2012), with a bright 'north polar cap' observed after 2014 (de Pater et al. 2015; Sromovsky et al. 2015; Toledo et al. 2018). By computing photometric brightness from Hubble imaging between August 1994 and October 2015, Karkoschka (2016) showed that both the changing view of Uranus in Fig. 9 and the real physical changes were modulating the brightness - darkening of high southern latitudes, and brightening of high northern latitudes.

What could be causing these changes at high latitudes?  $\text{CH}_4$  is strongly depleted at the poles so there is less absorption (Section 3.1.3), and although Toledo et al. (2018) suggested that temporal evolution of this

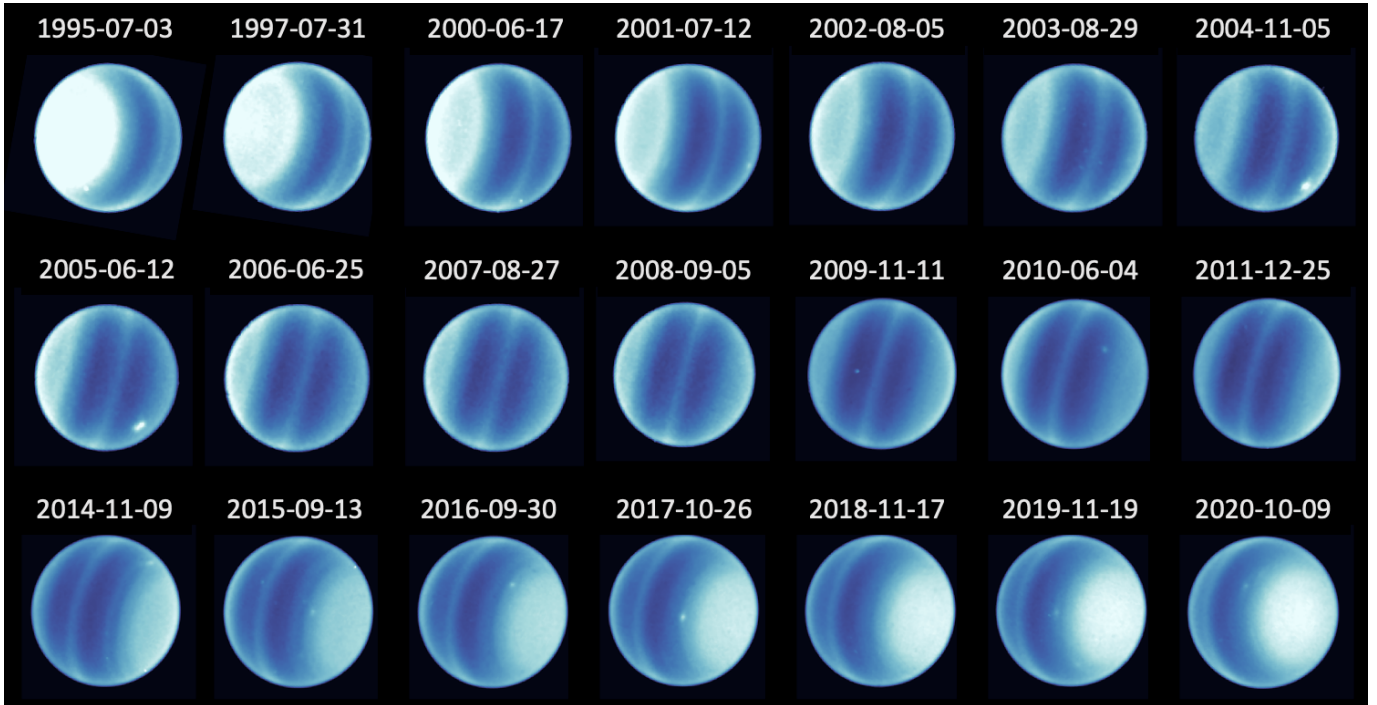


**Figure 9.** Hubble observations at 619 nm, a weak methane absorption band, showing the evolution of Uranus’ reflectivity over a quarter of a century, spanning mid-winter, spring equinox, and mid-spring in the northern hemisphere. Observations before 2009 were acquired by the WFPC2 instrument, observations after 2009 were acquired by the WFC3 instrument, largely by the Outer Planet Atmospheres Legacy (OPAL) programme since 2014.

‘methane hole’ could be responsible, [Sromovsky et al. \(2019\)](#) revealed that the polar  $\text{CH}_4$  was relatively stable over time, and suggest that increased scattering from seasonally-changing aerosols is required. There are problems with this, as the polar aerosols appear to be changing over short timescales in Fig. 9, so cannot be explained via long radiative ([Conrath et al. 1990](#)), photochemical ([Moses et al. 2018](#)), or microphysical processes (aerosol accumulation and sedimentation are slow processes that would produce a substantial seasonal lag, [Toledo et al. 2019](#)). It seems likely that tropospheric and stratospheric circulation must be playing a role ([Fletcher et al. 2020a](#)), again highlighting the complexity of the coupled circulation, chemistry, and clouds of Uranus’ atmosphere.

Long-term monitoring of visible albedo (472 and 551 nm) between 1972 and 2016 ([Lockwood and Thompson 1999](#); [Hammel et al. 2007](#); [Lockwood 2019](#)), and broadband B and V photometry from 1950 to 1966 ([Lockwood and Jerzykiewicz 2006](#)), are consistent with the geometric effects as the bright polar caps and collars come in and out of view, but also suggest more subtle, secular variations in brightness. In particular, Uranus’ reflectivity is related to the 11-year solar cycle, both through changing levels of UV (which could be modulating the colours of aerosols via a ‘tanning’ process, [Baines and](#)

[Smith 1990](#)), and also through the ion-induced nucleation generated by galactic cosmic rays ([Aplin and Fischer 2017](#); [Aplin et al. 2020](#)). These studies highlight the value of long-term Earth-based observations, to provide temporal context to short-lived spacecraft missions.

### 3.5. Connections

#### 3.5.1. Connection to the Interior

Although this review is focused on Uranus’ atmosphere, it cannot be considered in isolation from the deeper interior, and the external charged particle environment. It is not immediately clear where an Ice Giant atmosphere (molecular envelope) ends, and its interior or icy mantle begins. Differential rotation due to zonal winds appears to be restricted to the outermost 1000 km of Uranus’ 25559 km equatorial radius (i.e., the outer 4% down to  $\sim 2$  kbar, [Kaspi et al. 2013](#)). Deeper down at  $\sim 20$  kbar and 1200 K, is it possible that  $\text{H}_2\text{O}$  is insoluble in  $\text{H}_2$  ([Bali et al. 2013](#)), leading to the formation of a liquid water ocean at tens of kilobars ([Bailey and Stevenson 2015](#)). This immiscibility can lead to sharp interfaces, or an ocean surface, within the interior ([Bailey and Stevenson 2021](#)). This ocean would transition from being non-conducting to ionic/superionic at hundreds of kilobars, and could be responsible for removing  $\text{NH}_3$  by dissolution to explain the low N/S ratio de-



tected in the atmosphere (Section 2). The generation of Uranus’ internal dynamo (Ness et al. 1986) may be associated with convection in the partially dissociated fluid water layers (Redmer et al. 2011; Soderlund et al. 2013), and appreciable conductivity can be achieved at 20-30% of the radii below the surface (Soderlund and Stanley 2020). Dynamo simulations predict large-scale circulation in this watery layer, with equatorial upwelling and, depending on the thickness of the convecting layer, polar circulation cells (Soderlund et al. 2013), although it is unclear how this might relate to the circulation in the molecular envelope in Section 3.1. At even greater depths, high-pressure laboratory experiments suggest that water could form a thick superionic ‘icy mantle’, creating a solid-phase viscous lattice of oxygen ions surrounded by a sea of free hydrogen (Wilson et al. 2013; Millot et al. 2018, 2019).

These substantial transitions between exotic phases of matter in Uranus’ interior could lead to inhibition of convection and retention of interior heat (e.g., Hubbard et al. 1995), significantly influencing the thermal evolution of Uranus (Fortney et al. 2011). Indeed, different rates of hydrogen-water demixing, due to  $\text{H}_2\text{O}$  immiscibility and the formation of a water ocean, could explain the very different heat flow on Uranus compared to Neptune (Bailey and Stevenson 2021). Furthermore, the presence of these transitions could successfully decouple motions in the observable ‘dry’ atmosphere from those in the deeper, water-rich interior oceans. However, Helled et al. (2020) provide a cautionary note that we still do not know the bulk oxygen content of Uranus, to the extent that it might instead be dominated by rocky materials rather than water, and implying that the oft-used term ‘Ice Giant’ may be misleading.

### 3.5.2. Connection to the Exterior

The circulation and chemistry of the middle atmosphere (e.g., the stratosphere) will also be intricately connected to processes shaping the upper atmosphere (e.g., ionosphere/thermosphere), above the homopause where hydrogen dominates. Weak solar heating alone cannot explain the high temperatures of Uranus’ thermosphere (Herbert et al. 1987), a deficit known as the ‘energy crisis,’ and contributions from auroral heating and potentially the breaking of vertically-propagating waves have been invoked to close the gap between observations and expectations. Extreme UV radiation, or impact ionisation from the aurora, produces the  $\text{H}_3^+$  ion, which was first detected on Uranus in 1992 (Trafton et al. 1993), and has been monitored ever since, revealing a long-term cooling of Uranus’ thermosphere over three decades (Melin et al. 2019). That  $\text{H}_3^+$  produc-

tion appears to be efficient on Uranus, but not Neptune, may be related to the weak atmospheric mixing and low homopause height. The thermospheric cooling trend appears to be decoupled from Uranus’ geometric season (i.e., it did not change after the 2007 equinox), but might be explained by a ‘magnetic season:’ differing amounts of Joule heating at different points in the planet’s orbit, or changes to the homopause height with time, or a hemispherically asymmetric homopause that changes the  $\text{H}_3^+$  density on the hemisphere visible from Earth (see Melin 2020, for a review). Whether this redistribution of energy in Uranus’ upper atmosphere has any implications for the energy balance, circulation, and chemistry of the stratosphere remains to be seen.

Auroral emission has been observed via excitation of H Lyman- $\alpha$  and  $\text{H}_2$  bands due to precipitating energetic particles (Lamy 2020). These are located at magnetic poles tilted from the rotational axis by  $\sim 60^\circ$ , as observed by Voyager UVS (Herbert et al. 1987) and later Hubble (Lamy et al. 2012, 2017). Auroral brightening has also been tentatively detected in the infrared via  $\text{H}_3^+$  emission (Thomas et al. 2020). On Jupiter ion-neutral chemistry related to the aurora can lead to a unique balance of stratospheric chemicals and aerosols in the polar domain, so future observations could test whether this is also true on Uranus, given the mid-latitude location of the magnetic poles.

## 4. CONCLUSIONS AND OUTSTANDING QUESTIONS

This review should dispel any remaining myths about Uranus’ atmosphere held over from the first Voyager images, revealing it to be an extreme laboratory for testing our understanding of the processes shaping planetary atmospheres. Indeed, Uranus’ atmosphere occupies a unique regime in parameter space:

- An intermediate-sized world rotating a rate slower than Jupiter but faster than Earth, with implications for the banded structure (Section 3.1);
- A hydrogen-rich molecular envelope with a bulk that is substantially enriched in heavy materials (volatiles and rocks) and strong equator-to-pole gradients in condensables (Sections 2 and 3.1);
- The unusual seasonal effects due to both the extreme axial tilt, weak sunlight, and negligible internal heat, perhaps sequestered by strong layering associated with phase transitions in watery oceans and icy mantles at tens and hundreds of kilobars (Sections 3.4 and 3.5);
- The low temperatures and weak vertical mixing meaning that photochemistry occurs in a high-



pressure, low-temperature regime, and a low homopause permitting the formation of an extensive ionosphere (Section 3.3;

- The small-scale cloud phenomena, episodic outbursts, equatorial waves, and moist convective activity operating at shallow and accessible depths, potentially driven by CH<sub>4</sub> condensation and ortho/para-H<sub>2</sub> interconversion (Section 3.2;
- The stabilising effects of phase transitions implying layered tiers of circulation patterns and convection, potentially decoupled from one another as a function of depth (Sections 3.1 and 3.2).

The above list is not intended to be exhaustive, but provides numerous compelling reasons for future exploration of Uranus, both as a fascinating object in its own right, but also as one of our closest and best examples of a class of worlds that might be commonplace, being only slightly larger than the ‘sub-Neptunes’ that currently dominate the census of exoplanets (Fulton and Petigura 2018). Uranus and Neptune will be the last remaining class of Solar System planet to have a dedicated orbital explorer, and international efforts are under way to develop an ambitious mission to Uranus in the coming decades, combining an orbital tour with *in situ* descent probes (Arridge et al. 2012; Mousis et al. 2018; Hofstadter et al. 2019; Fletcher et al. 2020b; Simon et al. 2020; Fletcher et al. 2020d).

Such a mission would be transformative for our understanding of Uranus, in the same way as Cassini, Galileo, and Juno transformed our understanding of the Gas Giants. Key questions to be addressed by such a mission, supported by Earth-based multi-spectral remote sensing, are as follows:

- What is the bulk composition of Uranus’ interior, particularly the ice-to-rock ratio, elemental abundances (including noble gases) and isotopic ratios? How well does the atmospheric composition represent the bulk, and how do water-rich oceans/mantles influence the observed composition? These will provide crucial constraints on Uranus’ formation and migration by revealing which reservoirs were available to the forming Uranus.
- What are the dynamical, meteorological, and chemical impacts of the negligible planetary lumi-

osity, weak vertical mixing, and Uranus’ extreme seasons, and how do atmospheric phenomena differ between Uranus and Neptune?

- What is the large-scale circulation of Uranus’ atmosphere, how deep does it penetrate into the interior and is it coupled to interior motions, and do stable layers produce decoupled tiers of circulation and convection?
- What is the role of moist convection and precipitation in Uranus’ hydrogen-dominated atmosphere, and how do updrafts overcome the static stability of the cloud bases?
- Does Uranus really have no appreciable internal heat, or is this merely trapped, or time variable? If so, what does this imply about Uranus’ thermal evolution, and why does it differ from Neptune?
- What are the sources of energy responsible for heating the middle and upper atmosphere of Uranus, and how does the ionosphere couple the atmosphere to the external magnetosphere?
- How does Uranus’ atmosphere evolve with time? Is the banded structure relatively stable, or do the winds, cloud features, and albedo patterns shift over time? How do vortices form, migrate, and interact in Uranus’ atmosphere?

To date, progress in addressing these questions has been hampered by the extreme challenge of observing Uranus in the decades since Voyager. Nevertheless, this review demonstrates how far we have come in developing our understanding of this unusual world, and whets our appetite for exciting new discoveries in the coming decades.

Fletcher is supported by a European Research Council Consolidator Grant (under the European Union’s Horizon 2020 research and innovation programme, grant agreement No 723890) at the University of Leicester. I would like to extend my thanks to Michael Roman for providing the artwork for Fig. 4, Ricardo Hueso for Fig. 5, to Julianne Moses for providing the model data plotted in Fig. 8, to Glenn Orton for providing guidance for spectroscopy in Fig. 3, and to Helmut Feuchtgruber and Martin Burgdorf for allowing me to show the ISO observations in Fig. 3.

## REFERENCES

Alexander, A.F.O., 1965. The planet Uranus; a history of observation, theory, and discovery.

Ali-Dib, M., Mousis, O., Petit, J.M., Lunine, J.I., 2014. The Measured Compositions of Uranus and Neptune from their Formation on the CO Ice Line. *Astrophys. J.* 793, 9. doi:<https://doi.org/10.1088/0004-637X/793/1/9>, [arXiv:1407.2568](https://arxiv.org/abs/1407.2568).

- Aplin, K.L., Fischer, G., 2017. Lightning detection in planetary atmospheres. *Weather* 72, 46–50.  
doi:<https://doi.org/10.1002/wea.2817>,  
arXiv:1606.03285.
- Aplin, K.L., Fischer, G., Nordheim, T.A., Konovalenko, A., Zakharenko, V., Zarka, P., 2020. Atmospheric Electricity at the Ice Giants. *Space Sci. Rev.* 216, 26.  
doi:<https://doi.org/10.1007/s11214-020-00647-0>,  
arXiv:1907.07151.
- Arridge, C.S., Agnor, C.B., André, N., Baines, K.H., Fletcher, L.N., Gautier, D., Hofstadter, M.D., Jones, G.H., Lamy, L., Langevin, Y., Mousis, O., Nettelmann, N., Russell, C.T., Stallard, T., Tiscareno, M.S., Tobie, G., Bacon, A., Chaloner, C., Guest, M., Kemble, S., Peacocke, L., Achilleos, N., Andert, T.P., Banfield, D., Barabash, S., Barthelémy, M., Bertucci, C., Brandt, P., Cecconi, B., Chakrabarti, S., Cheng, A.F., Christensen, U., Christou, A., Coates, A.J., Collinson, G., Cooper, J.F., Courtin, R., Dougherty, M.K., Ebert, R.W., Entradas, M., Fazakerley, A.N., Fortney, J.J., Galand, M., Gustin, J., Hedman, M., Helled, R., Henri, P., Hess, S., Holme, R., Karatekin, Ö., Krupp, N., Leisner, J., Martin-Torres, J., Masters, A., Melin, H., Miller, S., Müller-Wodarg, I., Noyelles, B., Paranicas, C., de Pater, I., Pätzold, M., Prangé, R., Quémerais, E., Roussos, E., Rymer, A.M., Sánchez-Lavega, A., Saur, J., Sayanagi, K.M., Schenk, P., Schubert, G., Sergis, N., Sohl, F., Sittler, E.C., Teanby, N.A., Tellmann, S., Turtle, E.P., Vinatier, S., Wahlund, J.E., Zarka, P., 2012. Uranus Pathfinder: exploring the origins and evolution of Ice Giant planets. *Experimental Astronomy* 33, 753–791.  
doi:<https://doi.org/10.1007/s10686-011-9251-4>.
- Asplund, M., Grevesse, N., Sauval, A.J., Scott, P., 2009. The Chemical Composition of the Sun. *Annual Rev. Astron. & Astrophys.* 47, 481–522.  
doi:<https://doi.org/10.1146/annurev.astro.46.060407.145222>,  
arXiv:0909.0948.
- Atreya, S.K., Hofstadter, M.H., In, J.H., Mousis, O., Reh, K., Wong, M.H., 2020. Deep Atmosphere Composition, Structure, Origin, and Exploration, with Particular Focus on Critical in situ Science at the Icy Giants. *Space Science Reviews* 216, 18.  
doi:<https://doi.org/10.1007/s11214-020-0640-8>.
- Atreya, S.K., Ponthieu, J.J., 1983. Photolysis of methane and the ionosphere of Uranus. *Plan. & Space Sci.* 31, 939–944.  
doi:[https://doi.org/10.1016/0032-0633\(83\)90149-6](https://doi.org/10.1016/0032-0633(83)90149-6).
- Atreya, S.K., Sandel, B.R., Romani, P.N., 1991. Photochemistry and vertical mixing. Arizona Press. pp. 110–146.
- Atreya, S.K., Wong, A.S., 2005. Coupled Clouds and Chemistry of the Giant Planets – A Case for Multiprobes. *Space Sci. Rev.* 116, 121–136.  
doi:<https://doi.org/10.1007/s11214-005-1951-5>.
- Bailey, E., Stevenson, D.J., 2015. Modeling Ice Giant Interiors Using Constraints on the H<sub>2</sub>-H<sub>2</sub>O Critical Curve, in: AGU Fall Meeting Abstracts, pp. P31G–03.
- Bailey, E., Stevenson, D.J., 2021. Thermodynamically Governed Interior Models of Uranus and Neptune. *The Planetary Science Journal* 2, 64.  
doi:<https://doi.org/10.3847/PSJ/abd1e0>,  
arXiv:2012.04166.
- Baines, K.H., Mickelson, M.E., Larson, L.E., Ferguson, D.W., 1995. The abundances of methane and ortho/para hydrogen on Uranus and Neptune: Implications of New Laboratory 4-0 H<sub>2</sub> quadrupole line parameters. *Icarus* 114, 328–340.  
doi:<https://doi.org/10.1006/icar.1995.1065>.
- Baines, K.H., Smith, H.W., 1990. The atmospheric structure and dynamical properties of Neptune derived from ground-based and IUE spectrophotometry. *Icarus* 85, 65–108.  
doi:[https://doi.org/10.1016/0019-1035\(90\)90104-H](https://doi.org/10.1016/0019-1035(90)90104-H).
- Bali, E., Audéat, A., Keppler, H., 2013. Water and hydrogen are immiscible in Earth’s mantle. *Nature* 495, 220–222. doi:<https://doi.org/10.1038/nature11908>.
- Bishop, J., Atreya, S.K., Herbert, F., Romani, P., 1990. Reanalysis of Voyager 2 UVS occultations at Uranus - Hydrocarbon mixing ratios in the equatorial stratosphere. *Icarus* 88, 448–464.  
doi:[https://doi.org/10.1016/0019-1035\(90\)90094-P](https://doi.org/10.1016/0019-1035(90)90094-P).
- Bolton, S.J., Adriani, A., Adumitroaie, V., Allison, M., Anderson, J., Atreya, S., Bloxham, J., Brown, S., Connerney, J.E.P., DeJong, E., Folkner, W., Gautier, D., Grassi, D., Gulkis, S., Guillot, T., Hansen, C., Hubbard, W.B., Iess, L., Ingersoll, A., Janssen, M., Jorgensen, J., Kaspi, Y., Levin, S.M., Li, C., Lunine, J., Miguel, Y., Mura, A., Orton, G., Owen, T., Ravine, M., Smith, E., Steffes, P., Stone, E., Stevenson, D., Thorne, R., Waite, J., Durante, D., Ebert, R.W., Greathouse, T.K., Hue, V., Parisi, M., Szalay, J.R., Wilson, R., 2017. Jupiter’s interior and deep atmosphere: The initial pole-to-pole passes with the Juno spacecraft. *Science* 356, 821–825.  
doi:<https://doi.org/10.1126/science.aal2108>.
- Burgdorf, M., Orton, G., van Cleve, J., Meadows, V., Houck, J., 2006. Detection of new hydrocarbons in Uranus’ atmosphere by infrared spectroscopy. *Icarus* 184, 634–637.  
doi:<https://doi.org/10.1016/j.icarus.2006.06.006>.

- Cavalié, T., Moreno, R., Lellouch, E., Hartogh, P., Venot, O., Orton, G.S., Jarchow, C., Encrenaz, T., Selsis, F., Hersant, F., Fletcher, L.N., 2013. First submillimeter observation of CO in the stratosphere of Uranus. *Astronomy and Astrophysics* accepted.
- Cavalié, T., Venot, O., Miguel, Y., Fletcher, L.N., Wurz, P., Mousis, O., Bounaceur, R., Hue, V., Leconte, J., Dobrijevic, M., 2020. The Deep Composition of Uranus and Neptune from In Situ Exploration and Thermochemical Modeling. *Space Sci. Rev.* 216, 58. doi:<https://doi.org/10.1007/s11214-020-00677-8>, arXiv:2004.13987.
- Cavalié, T., Venot, O., Selsis, F., Hersant, F., Hartogh, P., Leconte, J., 2017. Thermochemistry and vertical mixing in the tropospheres of Uranus and Neptune: How convection inhibition can affect the derivation of deep oxygen abundances. *Icarus* 291, 1–16. doi:<https://doi.org/10.1016/j.icarus.2017.03.015>, arXiv:1703.04358.
- Conrath, B., Gautier, D., Owen, T., Samuelson, R., 1993. Constraints on N<sub>2</sub> in Neptune’s Atmosphere from Voyager Measurements. *Icarus* 101, 168–172.
- Conrath, B., Hanel, R., Gautier, D., Marten, A., Lindal, G., 1987. The helium abundance of Uranus from Voyager measurements. *Journal of Geophysical Research* 92, 15003–15010. doi:<https://doi.org/10.1029/JA092iA13p15003>.
- Conrath, B.J., Gierasch, P.J., Leroy, S.S., 1990. Temperature and circulation in the stratosphere of the outer planets. *Icarus* 83, 255–281. doi:[https://doi.org/10.1016/0019-1035\(90\)90068-K](https://doi.org/10.1016/0019-1035(90)90068-K).
- Conrath, B.J., Gierasch, P.J., Ustinov, E.A., 1998. Thermal Structure and Para Hydrogen Fraction on the Outer Planets from Voyager IRIS Measurements. *Icarus* 135, 501–517. doi:<https://doi.org/10.1006/icar.1998.6000>.
- de Kleer, K., Luszcz-Cook, S., de Pater, I., Ádámkóvics, M., Hammel, H.B., 2015. Clouds and aerosols on Uranus: Radiative transfer modeling of spatially-resolved near-infrared Keck spectra. *Icarus* 256, 120–137. doi:<https://doi.org/10.1016/j.icarus.2015.04.021>.
- de Pater, I., 1991. The Significance of Radio Observations for Planets. *Physics Reports* , 1–50.
- de Pater, I., Butler, B., Sault, R.J., Moullet, A., Moeckel, C., Tollefson, J., de Kleer, K., Gurwell, M., Milam, S., 2018. Potential for Solar System Science with the ngVLA. *Science with a Next Generation Very Large Array* 517, 49. arXiv:1810.08521.
- de Pater, I., Fletcher, L.N., Luszcz-Cook, S., DeBoer, D., Butler, B., Hammel, H.B., Sitko, M.L., Orton, G., Marcus, P.S., 2014. Neptune’s global circulation deduced from multi-wavelength observations. *Icarus* 237, 211–238. doi:<https://doi.org/10.1016/j.icarus.2014.02.030>.
- de Pater, I., Gibbard, S.G., Macintosh, B.A., Roe, H.G., Gavel, D.T., Max, C.E., 2002. Keck Adaptive Optics Images of Uranus and Its Rings. *Icarus* 160, 359–374. doi:<https://doi.org/10.1006/icar.2002.6966>.
- de Pater, I., Gulikis, S., 1988. VLA observations of Uranus at 1.3–20 CM. *Icarus* 75, 306–323. doi:[https://doi.org/10.1016/0019-1035\(88\)90007-3](https://doi.org/10.1016/0019-1035(88)90007-3).
- de Pater, I., Sromovsky, L.A., Fry, P.M., Hammel, H.B., Baranec, C., Sayanagi, K.M., 2015. Record-breaking storm activity on Uranus in 2014. *Icarus* 252, 121–128. doi:<https://doi.org/10.1016/j.icarus.2014.12.037>, arXiv:1501.01309.
- de Pater, I., Sromovsky, L.A., Hammel, H.B., Fry, P.M., LeBeau, R.P., Rages, K., Showalter, M., Matthews, K., 2011. Post-equinox observations of Uranus: Berg’s evolution, vertical structure, and track towards the equator. *Icarus* 215, 332–345. doi:<https://doi.org/10.1016/j.icarus.2011.06.022>.
- DeBoer, D.R., Steffes, P.G., 1994. Laboratory Measurements of the Microwave Properties of H<sub>2</sub>S under Simulated Jovian Conditions with an Application to Neptune. *Icarus* 109, 352–366. doi:<https://doi.org/10.1006/icar.1994.1099>.
- DeBoer, D.R., Steffes, P.G., 1996. Estimates of the Tropospheric Vertical Structure of Neptune Based on Microwave Radiative Transfer Studies. *Icarus* 123, 324–335. doi:<https://doi.org/10.1006/icar.1996.0161>.
- Dobrijevic, M., Cavalié, T., Hébrard, E., Billebaud, F., Hersant, F., Selsis, F., 2010. Key reactions in the photochemistry of hydrocarbons in Neptune’s stratosphere. *Plan. & Space Sci.* 58, 1555–1566. doi:<https://doi.org/10.1016/j.pss.2010.07.024>.
- Encrenaz, T., Feuchtgruber, H., Atreya, S.K., Bezaud, B., Lellouch, E., Bishop, J., Edgington, S., Degraauw, T., Griffin, M., Kessler, M.F., 1998. ISO observations of Uranus: The stratospheric distribution of C<sub>2</sub>H<sub>2</sub> and the eddy diffusion coefficient. *Astron. Astrophys* 333, L43–L46.
- Encrenaz, T., Lellouch, E., Drossart, P., Feuchtgruber, H., Orton, G.S., Atreya, S.K., 2004. First detection of CO in Uranus. *Astron. Astrophys* 413, L5–L9. doi:<https://doi.org/10.1051/0004-6361:20034637>.

- Encrenaz, T., Schulz, B., Drossart, P., Lellouch, E., Feuchtgruber, H., Atreya, S.K., 2000. The ISO spectra of Uranus and Neptune between 2.5 and 4.2  $\mu\text{m}$ : constraints on albedos and  $\text{H}_3^+$ . *Astron. Astrophys* 358, L83–L87.
- Fegley, Jr., B., Lodders, K., 1994. Chemical models of the deep atmospheres of Jupiter and Saturn. *Icarus* 110, 117–154. doi:<https://doi.org/10.1006/icar.1994.1111>.
- Fegley, B., J., Prinn, R.G., 1986. Chemical Models of the Deep Atmosphere of Uranus. *Astrophys. J.* 307, 852. doi:<https://doi.org/10.1086/164472>.
- Feuchtgruber, H., Lellouch, E., de Graauw, T., Bezaud, B., Encrenaz, T., Griffin, M., 1997. External supply of oxygen to the atmospheres of giant planets. *Nature* 389, 159–162.
- Feuchtgruber, H., Lellouch, E., Orton, G., de Graauw, T., Vandenbussche, B., Swinyard, B., Moreno, R., Jarchow, C., Billebaud, F., Cavalié, T., Sidher, S., Hartogh, P., 2013. The D/H ratio in the atmospheres of Uranus and Neptune from Herschel-PACS observations. *Astron. Astrophys* 551, A126. doi:<https://doi.org/10.1051/0004-6361/201220857>, [arXiv:1301.5781](https://arxiv.org/abs/1301.5781).
- Flasar, F.M., Conrath, B.J., Pirraglia, J.A., Gierasch, P.J., 1987. Voyager infrared observations of Uranus' atmosphere - Thermal structure and dynamics. *Journal of Geophysical Research* 92, 15011–15018. doi:<https://doi.org/10.1029/JA092iA13p15011>.
- Fletcher, L.N., de Pater, I., Orton, G.S., Hofstadter, M.D., Irwin, P.G.J., Roman, M.T., Toledo, D., 2020a. Ice Giant Circulation Patterns: Implications for Atmospheric Probes. *Space Science Reviews* 216, 21. doi:<https://doi.org/10.1007/s11214-020-00646-1>, [arXiv:1907.02901](https://arxiv.org/abs/1907.02901).
- Fletcher, L.N., Helled, R., Roussos, E., Jones, G., Charnoz, S., André, N., Andrews, D., Bannister, M., Bunce, E., Cavalié, T., Ferri, F., Fortney, J., Grassi, D., Griton, L., Hartogh, P., Hueso, R., Kaspi, Y., Lamy, L., Masters, A., Melin, H., Moses, J., Mousis, O., Nettleman, N., Plainaki, C., Schmidt, J., Simon, A., Tobie, G., Tortora, P., Tosi, F., Turrini, D., 2020b. Ice Giant Systems: The scientific potential of orbital missions to Uranus and Neptune. *Plan. & Space Sci.* 191, 105030. doi:<https://doi.org/10.1016/j.pss.2020.105030>, [arXiv:1907.02963](https://arxiv.org/abs/1907.02963).
- Fletcher, L.N., Kaspi, Y., Guillot, T., Showman, A.P., 2020c. How Well Do We Understand the Belt/Zone Circulation of Giant Planet Atmospheres? *Space Science Reviews* 216, 30. doi:<https://doi.org/10.1007/s11214-019-0631-9>.
- Fletcher, L.N., Simon, A.A., Hofstadter, M.D., Arridge, C.S., Cohen, I.J., Masters, A., Mandt, K., Coustenis, A., 2020d. Ice giant system exploration in the 2020s: an introduction. *Philosophical Transactions of the Royal Society of London Series A* 378, 20190473. doi:<https://doi.org/10.1098/rsta.2019.0473>.
- Fortney, J.J., Ikoma, M., Nettelmann, N., Guillot, T., Marley, M.S., 2011. Self-consistent Model Atmospheres and the Cooling of the Solar System's Giant Planets. *ApJ* 729, 32. doi:<https://doi.org/10.1088/0004-637X/729/1/32>, [arXiv:1101.0606](https://arxiv.org/abs/1101.0606).
- Friedson, A.J., Gonzales, E.J., 2017. Inhibition of ordinary and diffusive convection in the water condensation zone of the ice giants and implications for their thermal evolution. *Icarus* 297, 160–178. doi:<https://doi.org/10.1016/j.icarus.2017.06.029>.
- Friedson, J., Ingersoll, A.P., 1987. Seasonal meridional energy balance and thermal structure of the atmosphere of Uranus: A radiative-convective-dynamical model. *Icarus* 69, 135–156. doi:[https://doi.org/10.1016/0019-1035\(87\)90010-8](https://doi.org/10.1016/0019-1035(87)90010-8).
- Fry, P.M., Sromovsky, L.A., de Pater, I., Hammel, H.B., Rages, K.A., 2012. Detection and Tracking of Subtle Cloud Features on Uranus. *Astronomical Journal* 143, 150. doi:<https://doi.org/10.1088/0004-6256/143/6/150>.
- Fulton, B.J., Petigura, E.A., 2018. The California-Kepler Survey. VII. Precise Planet Radii Leveraging Gaia DR2 Reveal the Stellar Mass Dependence of the Planet Radius Gap. *Astronomical Journal* 156, 264. doi:<https://doi.org/10.3847/1538-3881/aae828>, [arXiv:1805.01453](https://arxiv.org/abs/1805.01453).
- Gierasch, P.J., Conrath, B.J., 1987. Vertical temperature gradients on Uranus - Implications for layered convection. *Journal of Geophysical Research* 92, 15019–15029. doi:<https://doi.org/10.1029/JA092iA13p15019>.
- Guillot, T., 1995. Condensation of Methane, Ammonia, and Water and the Inhibition of Convection in Giant Planets. *Science* 269, 1697–1699. doi:<https://doi.org/10.1126/science.7569896>.
- Guillot, T., 2019. Uranus and Neptune are key to understand planets with hydrogen atmospheres. *arXiv e-prints*, [arXiv:1908.02092](https://arxiv.org/abs/1908.02092), [arXiv:1908.02092](https://arxiv.org/abs/1908.02092).
- Gulkis, S., Janssen, M.A., Olsen, E.T., 1978. Evidence for the depletion of ammonia in the Uranus atmosphere. *Icarus* 34, 10–19. doi:[https://doi.org/10.1016/0019-1035\(78\)90120-3](https://doi.org/10.1016/0019-1035(78)90120-3).



- Hammel, H.B., de Pater, I., Gibbard, S., Lockwood, G.W., Rages, K., 2005a. Uranus in 2003: Zonal winds, banded structure, and discrete features. *Icarus* 175, 534–545. doi:<https://doi.org/10.1016/j.icarus.2004.11.012>.
- Hammel, H.B., de Pater, I., Gibbard, S.G., Lockwood, G.W., Rages, K., 2005b. New cloud activity on Uranus in 2004: First detection of a southern feature at 2.2  $\mu\text{m}$ . *Icarus* 175, 284–288. doi:<https://doi.org/10.1016/j.icarus.2004.11.016>.
- Hammel, H.B., Rages, K., Lockwood, G.W., Karkoschka, E., de Pater, I., 2001. New Measurements of the Winds of Uranus. *Icarus* 153, 229–235. doi:<https://doi.org/10.1006/icar.2001.6689>.
- Hammel, H.B., Sitko, M.L., Lynch, D.K., Orton, G.S., Russell, R.W., Geballe, T.R., de Pater, I., 2007. Distribution of Ethane and Methane Emission on Neptune. *Astron. J.* 134, 637–641. doi:<https://doi.org/10.1086/519382>.
- Hammel, H.B., Stromovsky, L.A., Fry, P.M., Rages, K., Showalter, M., de Pater, I., van Dam, M.A., LeBeau, R.P., Deng, X., 2009. The Dark Spot in the atmosphere of Uranus in 2006: Discovery, description, and dynamical simulations. *Icarus* 201, 257–271. doi:<https://doi.org/10.1016/j.icarus.2008.08.019>.
- Helled, R., Nettelmann, N., Guillot, T., 2020. Uranus and Neptune: Origin, Evolution and Internal Structure. *Space Science Reviews* 216, 38. doi:<https://doi.org/10.1007/s11214-020-00660-3>, [arXiv:1909.04891](https://arxiv.org/abs/1909.04891).
- Henry, P., Henry, P., 1884. Decouvertes Nouvelles sur Uranus. *L’Astronomie* 3, 281–282.
- Herbert, F., Sandel, B.R., Yelle, R.V., Holberg, J.B., Broadfoot, A.L., Shemansky, D.E., Atreya, S.K., Romani, P.N., 1987. The upper atmosphere of Uranus - EUV occultations observed by Voyager 2. *Journal of Geophysical Research* 92, 15093–15109. doi:<https://doi.org/10.1029/JA092iA13p15093>.
- Hersant, F., Gautier, D., Lunine, J.I., 2004. Enrichment in volatiles in the giant planets of the Solar System. *Plan. & Space Sci.* 52, 623–641. doi:<https://doi.org/10.1016/j.pss.2003.12.011>.
- Herzberg, G., 1952. Spectroscopic evidence of molecular hydrogen in the atmospheres of Uranus and Neptune. *Astrophys. J.* 115, 337–340. doi:<https://doi.org/10.1086/145552>.
- Hofstadter, M., Simon, A., Atreya, S., Banfield, D., Fortney, J.J., Hayes, A., Hedman, M., Hospodarsky, G., Mandt, K., Masters, A., Showalter, M., Soderlund, K.M., Turrini, D., Turtle, E., Reh, K., Elliott, J., Arora, N., Petropoulos, A., Ice Giant Mission Study Team, 2019. Uranus and Neptune missions: A study in advance of the next Planetary Science Decadal Survey. *Plan. & Space Sci.* 177, 104680. doi:<https://doi.org/10.1016/j.pss.2019.06.004>.
- Hofstadter, M.D., Butler, B.J., 2003. Seasonal change in the deep atmosphere of Uranus. *Icarus* 165, 168–180. doi:[https://doi.org/10.1016/S0019-1035\(03\)00174-X](https://doi.org/10.1016/S0019-1035(03)00174-X).
- Hofstadter, M.D., Butler, B.J., Hammel, H.B., Klein, M.J., 2004. The Discovery of Radio-Bright Northern Latitudes on Uranus: Implications for Weather and Climate, in: AAS/Division for Planetary Sciences Meeting Abstracts #36, p. 05.09.
- Holton, J., 2004. An Introduction to Dynamic Meteorology. Academic press.
- Hubbard, W.B., Nellis, W.J., Mitchell, A.C., Holmes, N.C., Limaye, S.S., McCandless, P.C., 1991. Interior Structure of Neptune: Comparison with Uranus. *Science* 253, 648–651. doi:<https://doi.org/10.1126/science.253.5020.648>.
- Hubbard, W.B., Podolak, M., Stevenson, D.J., 1995. The interior of Neptune., in: Neptune and Triton, pp. 109–138.
- Hueso, R., Guillot, T., Sánchez-Lavega, A., 2020. Convective storms and atmospheric vertical structure in Uranus and Neptune. *Philosophical Transactions of the Royal Society of London Series A* 378, 20190476. doi:<https://doi.org/10.1098/rsta.2019.0476>.
- Hueso, R., Sánchez-Lavega, A., 2019. Atmospheric Dynamics and Vertical Structure of Uranus and Neptune’s Weather Layers. *Space Science Reviews* 215, 52. doi:<https://doi.org/10.1007/s11214-019-0618-6>.
- Ingersoll, A.P., J., G.P., D., B., Vasavada, A.R., Galileo Imaging Team, 2000. Moist convection as an energy source for the large-scale motions in Jupiter’s atmosphere. *Nature* 403, 630–632. doi:<https://doi.org/10.1038/35001021>.
- Irwin, P.G.J., Fletcher, L.N., Read, P.L., Tice, D., de Pater, I., Orton, G.S., Teanby, N.A., Davis, G.R., 2016. Spectral analysis of Uranus’ 2014 bright storm with VLT/SINFONI. *Icarus* 264, 72–89. doi:<https://doi.org/10.1016/j.icarus.2015.09.010>, [arXiv:1510.02274](https://arxiv.org/abs/1510.02274).

- Irwin, P.G.J., Teanby, N.A., Davis, G.R., 2009. Vertical cloud structure of Uranus from UKIRT/UIST observations and changes seen during Uranus' northern spring equinox from 2006 to 2008. *Icarus* 203, 287–302. doi:<https://doi.org/10.1016/j.icarus.2009.05.003>.
- Irwin, P.G.J., Teanby, N.A., Davis, G.R., 2010. Revised vertical cloud structure of Uranus from UKIRT/UIST observations and changes seen during Uranus' Northern Spring Equinox from 2006 to 2008: Application of new methane absorption data and comparison with Neptune. *Icarus* 208, 913–926. doi:<https://doi.org/10.1016/j.icarus.2010.03.017>.
- Irwin, P.G.J., Teanby, N.A., Davis, G.R., Fletcher, L.N., Orton, G.S., Calcutt, S.B., Tice, D.S., Hurley, J., 2012. Further seasonal changes in Uranus' cloud structure observed by Gemini-North and UKIRT. *Icarus* 218, 47–55. doi:<https://doi.org/10.1016/j.icarus.2011.12.001>.
- Irwin, P.G.J., Toledo, D., Garland, R., Teanby, N.A., Fletcher, L.N., Orton, G.A., Bézard, B., 2018. Detection of hydrogen sulfide above the clouds in Uranus's atmosphere. *Nature Astronomy* 2, 420–427. doi:<https://doi.org/10.1038/s41550-018-0432-1>.
- Irwin, P.G.J., Wong, M.H., Simon, A.A., Orton, G.S., Toledo, D., 2017. HST/WFC3 observations of Uranus' 2014 storm clouds and comparison with VLT/SINFONI and IRTF/Spex observations. *Icarus* 288, 99–119. doi:<https://doi.org/10.1016/j.icarus.2017.01.031>, [arXiv:1611.03257](https://arxiv.org/abs/1611.03257).
- Karkoschka, E., 1994. Spectrophotometry of the Jovian Planets and Titan at 300- to 1000-nm Wavelength: The Methane Spectrum. *Icarus* 111, 174–192. doi:<https://doi.org/10.1006/icar.1994.1139>.
- Karkoschka, E., 1997. Rings and Satellites of Uranus: Colorful and Not So Dark. *Icarus* 125, 348–363. doi:<https://doi.org/10.1006/icar.1996.5631>.
- Karkoschka, E., 1998. Clouds of High Contrast on Uranus. *Science* 280, 570. doi:<https://doi.org/10.1126/science.280.5363.570>.
- Karkoschka, E., 2001a. Comprehensive Photometry of the Rings and 16 Satellites of Uranus with the Hubble Space Telescope. *Icarus* 151, 51–68. doi:<https://doi.org/10.1006/icar.2001.6596>.
- Karkoschka, E., 2001b. Uranus' Apparent Seasonal Variability in 25 HST Filters. *Icarus* 151, 84–92. doi:<https://doi.org/10.1006/icar.2001.6599>.
- Karkoschka, E., 2015. Uranus' southern circulation revealed by Voyager 2: Unique characteristics. *Icarus* 250, 294–307. doi:<https://doi.org/10.1016/j.icarus.2014.12.003>.
- Karkoschka, E., 2016. HST Photometry of Uranus 1994–2015, in: AAS/Division for Planetary Sciences Meeting Abstracts #48, p. 514.03.
- Karkoschka, E., Tomasko, M., 2009. The haze and methane distributions on Uranus from HST-STIS spectroscopy. *Icarus* 202, 287–309. doi:<https://doi.org/10.1016/j.icarus.2009.02.010>.
- Kaspi, Y., Showman, A.P., Hubbard, W.B., Aharonson, O., Helled, R., 2013. Atmospheric confinement of jet streams on Uranus and Neptune. *Nature* 497, 344–347. doi:<https://doi.org/10.1038/nature12131>.
- Kegerreis, J.A., Eke, V.R., Gonnet, P., Korycansky, D.G., Massey, R.J., Schaller, M., Teodoro, L.F.A., 2019. Planetary giant impacts: convergence of high-resolution simulations using efficient spherical initial conditions and SWIFT. *Monthly Notices of the Royal Astronomical Society* 487, 5029–5040. doi:<https://doi.org/10.1093/mnras/stz1606>, [arXiv:1901.09934](https://arxiv.org/abs/1901.09934).
- Kuiper, G.P., 1949. New absorptions in the uranian atmosphere. *Astrophys. J.* 109, 540–541. doi:<https://doi.org/10.1086/145161>.
- Lamy, L., 2020. Auroral emissions from Uranus and Neptune. *Philosophical Transactions of the Royal Society of London Series A* 378, 00481. doi:<https://doi.org/10.1098/rsta.2019.0481>.
- Lamy, L., Prangé, R., Hansen, K.C., Clarke, J.T., Zarka, P., Cecconi, B., Abouadarham, J., André, N., Branduardi-Raymont, G., Gladstone, R., Barthélémy, M., Achilleos, N., Guio, P., Dougherty, M.K., Melin, H., Cowley, S.W.H., Stallard, T.S., Nichols, J.D., Ballester, G., 2012. Earth-based detection of Uranus' aurorae. *Geophysical Research Letters* 39, L07105. doi:<https://doi.org/10.1029/2012GL051312>.
- Lamy, L., Prangé, R., Hansen, K.C., Tao, C., Cowley, S.W.H., Stallard, T.S., Melin, H., Achilleos, N., Guio, P., Badman, S.V., Kim, T., Pogorelov, N., 2017. The aurorae of Uranus past equinox. *Journal of Geophysical Research (Space Physics)* 122, 3997–4008. doi:<https://doi.org/10.1002/2017JA023918>.
- Lara, L.M., Rodrigo, R., Moreno, R., Lampón, M., 2019. Analysis of the origin of water, carbon monoxide, and carbon dioxide in the Uranus atmosphere. *Astron. Astrophys* 621, A129. doi:<https://doi.org/10.1051/0004-6361/201732123>.

- Leconte, J., Selsis, F., Hersant, F., Guillot, T., 2017. Condensation-inhibited convection in hydrogen-rich atmospheres . Stability against double-diffusive processes and thermal profiles for Jupiter, Saturn, Uranus, and Neptune. *A&A* 598, A98.  
doi:<https://doi.org/10.1051/0004-6361/201629140>,  
arXiv:1610.05506.
- Lellouch, E., Moreno, R., Orton, G.S., Feuchtgruber, H., Cavalié, T., Moses, J.I., Hartogh, P., Jarchow, C., Sagawa, H., 2015. New constraints on the CH<sub>4</sub> vertical profile in Uranus and Neptune from Herschel observations. *Astron. Astrophys* 579, A121.  
doi:<https://doi.org/10.1051/0004-6361/201526518>.
- Li, C., Ingersoll, A.P., 2015. Moist convection in hydrogen atmospheres and the frequency of Saturn's giant storms. *Nature Geoscience* 8, 398–403.  
doi:<https://doi.org/10.1038/ngeo2405>.
- Li, C., Le, T., Zhang, X., Yung, Y.L., 2018. A high-performance atmospheric radiation package: With applications to the radiative energy budgets of giant planets. *JQSRT* 217, 353–362.  
doi:<https://doi.org/10.1016/j.jqsrt.2018.06.002>,  
arXiv:1806.02573.
- Lindal, G.F., Lyons, J.R., Sweetnam, D.N., Eshleman, V.R., Hinson, D.P., 1987. The atmosphere of Uranus - Results of radio occultation measurements with Voyager 2. *Journal of Geophysical Research* 92, 14987–15001.  
doi:<https://doi.org/10.1029/JA092iA13p14987>.
- Lockwood, G.W., 2019. Final compilation of photometry of Uranus and Neptune, 1972-2016. *Icarus* 324, 77–85.  
doi:<https://doi.org/10.1016/j.icarus.2019.01.024>.
- Lockwood, G.W., Jerzykiewicz, M., 2006. Photometric variability of Uranus and Neptune, 1950-2004. *Icarus* 180, 442–452.  
doi:<https://doi.org/10.1016/j.icarus.2005.09.009>.
- Lockwood, G.W., Thompson, D.T., 1999. Photometric Variability of Uranus, 1972-1996. *Icarus* 137, 2–12.  
doi:<https://doi.org/10.1006/icar.1998.6029>.
- Lodders, K., Palme, H., Gail, H.P., 2009. Abundances of the Elements in the Solar System. *Solar System, Landolt-Börnstein - Group VI Astronomy and Astrophysics* 4B, 712.  
doi:<https://doi.org/10.1007/978-3-540-88055-4-34>,  
arXiv:0901.1149.
- Lunine, J.I., 1993. The atmospheres of Uranus and Neptune. *Annual Rev. Astron. & Astrophys.* 31, 217–263.  
doi:<https://doi.org/10.1146/annurev.aa.31.090193.001245>.
- Massie, S.T., Hunten, D.M., 1982. Conversion of para and ortho hydrogen in the Jovian planets. *Icarus* 49, 213–226.  
doi:[https://doi.org/10.1016/0019-1035\(82\)90073-2](https://doi.org/10.1016/0019-1035(82)90073-2).
- Melin, H., 2020. The upper atmospheres of Uranus and Neptune. *Philosophical Transactions of the Royal Society of London Series A* 378, 20190478.  
doi:<https://doi.org/10.1098/rsta.2019.0478>,  
arXiv:2009.02071.
- Melin, H., Fletcher, L.N., Stallard, T.S., Miller, S., Trafton, L.M., Vervack, R., Moore, L., O'Donoghue, J., Geballe, T.R., Lamy, L., Tao, C., Chowdhury, N., 2019. Ground-based H<sub>3</sub><sup>+</sup> observations of Uranus: the long-term and the short-term. *Royal Society of London Philosophical Transactions Series A* .
- Millot, M., Coppari, F., Rygg, J.R., Correa Barrios, A., Hamel, S., Swift, D.C., Eggert, J.H., 2019. Nanosecond X-ray diffraction of shock-compressed superionic water ice. *Nature* 569, 251–255.  
doi:<https://doi.org/10.1038/s41586-019-1114-6>.
- Millot, M., Hamel, S., Rygg, J.R., Celliers, P.M., Collins, G.W., Coppari, F., Fratanduono, D.E., Jeanloz, R., Swift, D.C., Eggert, J.H., 2018. Experimental evidence for superionic water ice using shock compression. *Nature Physics* 14, 297–302.  
doi:<https://doi.org/10.1038/s41567-017-0017-4>.
- Molter, E.M., de Pater, I., Luszcz-Cook, S., Tollefson, J., Sault, R.J., Butler, B., de Boer, D., 2021. Tropospheric Composition and Circulation of Uranus with ALMA and the VLA. *The Planetary Science Journal* 2, 3.  
doi:<https://doi.org/10.3847/PSJ/abc48a>,  
arXiv:2010.11154.
- Moreno, R., Marten, A., Lellouch, E., 2009. Search for PH<sub>3</sub> in the Atmospheres of Uranus and Neptune at Millimeter Wavelength, in: *AAS/Division for Planetary Sciences Meeting Abstracts #41*, p. 28.02.
- Moses, J.I., Cavalié, T., Fletcher, L.N., Roman, M.T., 2020. Atmospheric chemistry on Uranus and Neptune. *Philosophical Transactions of the Royal Society of London Series A* 378, 20190477.  
doi:<https://doi.org/10.1098/rsta.2019.0477>,  
arXiv:2006.11367.
- Moses, J.I., Fletcher, L.N., Greathouse, T.K., Orton, G.S., Hue, V., 2018. Seasonal stratospheric photochemistry on Uranus and Neptune. *Icarus* 307, 124–145.  
doi:<https://doi.org/10.1016/j.icarus.2018.02.004>,  
arXiv:1803.10338.

- Moses, J.I., Fouchet, T., Bézard, B., Gladstone, G.R., Lellouch, E., Feuchtgruber, H., 2005. Photochemistry and diffusion in Jupiter's stratosphere: Constraints from ISO observations and comparisons with other giant planets. *Journal of Geophysical Research (Planets)* 110, E08001. doi:<https://doi.org/10.1029/2005JE002411>.
- Moses, J.I., Poppe, A.R., 2017. Dust ablation on the giant planets: Consequences for stratospheric photochemistry. *Icarus* 297, 33–58. doi:<https://doi.org/10.1016/j.icarus.2017.06.002>, arXiv:1706.04686.
- Mousis, O., Atkinson, D.H., Cavalié, T., Fletcher, L.N., Amato, M.J., Aslam, S., Ferri, F., Renard, J.B., Spilker, T., Venkatapathy, E., Wurz, P., Aplin, K., Coustenis, A., Deleuil, M., Dobrijevic, M., Fouchet, T., Guillot, T., Hartogh, P., Hewagama, T., Hofstadter, M.D., Hue, V., Hueso, R., Lebreton, J.P., Lellouch, E., Moses, J., Orton, G.S., Pearl, J.C., Sánchez-Lavega, A., Simon, A., Venot, O., Waite, J.H., Achterberg, R.K., Atreya, S., Billebaud, F., Blanc, M., Borget, F., Brugger, B., Charnoz, S., Chiavassa, T., Cottini, V., d'Hendecourt, L., Danger, G., Encrenaz, T., Goriuss, N.J.P., Jorda, L., Marty, B., Moreno, R., Morse, A., Nixon, C., Reh, K., Ronnet, T., Schmider, F.X., Sheridan, S., Sotin, C., Vernazza, P., Villanueva, G.L., 2018. Scientific rationale for Uranus and Neptune in situ explorations. *Plan. & Space Sci.* 155, 12–40. doi:<https://doi.org/10.1016/j.pss.2017.10.005>, arXiv:1708.00235.
- Müller, T.G., Balog, Z., Nielbock, M., Moreno, R., Klaas, U., Moór, A., Linz, H., Feuchtgruber, H., 2016. Far-infrared photometric observations of the outer planets and satellites with Herschel-PACS. *Astron. Astrophys* 588, A109. doi:<https://doi.org/10.1051/0004-6361/201527371>, arXiv:1602.05785.
- Ness, N.F., Acuna, M.H., Behannon, K.W., Burlaga, L.F., Connerney, J.E.P., Lepping, R.P., Neubauer, F.M., 1986. Magnetic Fields at Uranus. *Science* 233, 85–89. doi:<https://doi.org/10.1126/science.233.4759.85>.
- Orton, G.S., Aitken, D.K., Smith, C., Roche, P.F., Caldwell, J., Snyder, R., 1987. The spectra of Uranus and Neptune at 8–14 and 17–23 microns. *Icarus* 70, 1–12. doi:[https://doi.org/10.1016/0019-1035\(87\)90070-4](https://doi.org/10.1016/0019-1035(87)90070-4).
- Orton, G.S., Fletcher, L.N., Encrenaz, T., Leyrat, C., Roe, H.G., Fujiyoshi, T., Pantin, E., 2015. Thermal imaging of Uranus: Upper-tropospheric temperatures one season after Voyager. *Icarus* 260, 94–102. doi:<https://doi.org/10.1016/j.icarus.2015.07.004>.
- Orton, G.S., Fletcher, L.N., Moses, J.I., Mainzer, A.K., Hines, D., Hammel, H.B., Martin-Torres, F.J., Burgdorf, M., Merlet, C., Line, M.R., 2014a. Mid-infrared spectroscopy of Uranus from the Spitzer Infrared Spectrometer: 1. Determination of the mean temperature structure of the upper troposphere and stratosphere. *Icarus* 243, 494–513. doi:<https://doi.org/10.1016/j.icarus.2014.07.010>, arXiv:1407.2120.
- Orton, G.S., Moses, J.I., Fletcher, L.N., Mainzer, A.K., Hines, D., Hammel, H.B., Martin-Torres, J., Burgdorf, M., Merlet, C., Line, M.R., 2014b. Mid-infrared spectroscopy of Uranus from the Spitzer infrared spectrometer: 2. Determination of the mean composition of the upper troposphere and stratosphere. *Icarus* 243, 471–493. doi:<https://doi.org/10.1016/j.icarus.2014.07.012>, arXiv:1407.2118.
- Owen, T., Mahaffy, P., Niemann, H.B., Atreya, S., Donahue, T., Bar-Nun, A., de Pater, I., 1999. A low-temperature origin for the planetesimals that formed Jupiter. *Nature* 402, 269–270.
- Pearl, J.C., Conrath, B.J., Hanel, R.A., Pirraglia, J.A., Coustenis, A., 1990. The albedo, effective temperature, and energy balance of Uranus, as determined from Voyager IRIS data. *Icarus* 84, 12–28. doi:[https://doi.org/10.1016/0019-1035\(90\)90155-3](https://doi.org/10.1016/0019-1035(90)90155-3).
- Podolak, M., Helled, R., Schubert, G., 2019. Effect of non-adiabatic thermal profiles on the inferred compositions of Uranus and Neptune. *Monthly Notices of the Royal Astronomical Society* 487, 2653–2664. doi:<https://doi.org/10.1093/mnras/stz1467>, arXiv:1905.09099.
- Rages, K., Pollack, J.B., Tomasko, M.G., Doose, L.R., 1991. Properties of scatterers in the troposphere and lower stratosphere of Uranus based on Voyager imaging data. *Icarus* 89, 359–376. doi:[https://doi.org/10.1016/0019-1035\(91\)90183-T](https://doi.org/10.1016/0019-1035(91)90183-T).
- Rages, K.A., Hammel, H.B., Friedson, A.J., 2004. Evidence for temporal change at Uranus' south pole. *Icarus* 172, 548–554. doi:<https://doi.org/10.1016/j.icarus.2004.07.009>.
- Rayner, J.T., Cushing, M.C., Vacca, W.D., 2009. The Infrared Telescope Facility (IRTF) Spectral Library: Cool Stars. *ApJ Supplement* 185, 289–432. doi:<https://doi.org/10.1088/0067-0049/185/2/289>, arXiv:0909.0818.



- Redmer, R., Mattsson, T.R., Nettelmann, N., French, M., 2011. The phase diagram of water and the magnetic fields of Uranus and Neptune. *Icarus* 211, 798–803. doi:<https://doi.org/10.1016/j.icarus.2010.08.008>.
- Roman, M.T., Banfield, D., Gierasch, P.J., 2018. Aerosols and methane in the ice giant atmospheres inferred from spatially resolved, near-infrared spectra: I. Uranus, 2001–2007. *Icarus* 310, 54–76. doi:<https://doi.org/10.1016/j.icarus.2017.10.036>, [arXiv:1710.09866](https://arxiv.org/abs/1710.09866).
- Roman, M.T., Fletcher, L.N., Orton, G.S., Rowe-Gurney, N., Irwin, P.G.J., 2020. Uranus in Northern Midspring: Persistent Atmospheric Temperatures and Circulations Inferred from Thermal Imaging. *Astronomical Journal* 159, 45. doi:<https://doi.org/10.3847/1538-3881/ab5dc7>, [arXiv:1911.12830](https://arxiv.org/abs/1911.12830).
- Romani, P.N., Bishop, J., Bezdard, B., Atreya, S., 1993. Methane photochemistry on Neptune - Ethane and acetylene mixing ratios and haze production. *Icarus* 106, 442. doi:<https://doi.org/10.1006/icar.1993.1184>.
- Rowe-Gurney, N., Fletcher, L.N., Orton, G.S., Roman, M.T., Mainzer, A., Moses, J.I., de Pater, I., Irwin, P.G.J., 2021. Longitudinal Variations in the Stratosphere of Uranus from the Spitzer Infrared Spectrometer. *Icarus*, in press .
- Safronov, V.S., 1966. Sizes of the largest bodies falling onto the planets during their formation. *Sov. Astron.* 9, 987–991.
- Sánchez-Lavega, A., Pérez-Hoyos, S., Hueso, R., 2004. Clouds in planetary atmospheres: A useful application of the Clausius-Clapeyron equation. *American Journal of Physics* 72, 767–774. doi:<https://doi.org/10.1119/1.1645279>.
- Sanchez-Lavega, A., Sromovsky, L.A., Showman, A.P., Del Genio, A.D., Young, R.M.B., Hueso, R., García-Melendo, E., Kaspi, Y., Orton, G.S., Barrado-Izagirre, N., Choi, D.S., Barbara, J.M., 2019. *Gas Giants*. Cambridge University Press. chapter 4.
- Showman, A.P., de Pater, I., 2005. Dynamical implications of Jupiter’s tropospheric ammonia abundance. *Icarus* 174, 192–204. doi:<https://doi.org/10.1016/j.icarus.2004.10.004>.
- Simon, A.A., Fletcher, L.N., Arridge, C., Atkinson, D., Coustenis, A., Ferri, F., Hofstadter, M., Masters, A., Mousis, O., Reh, K., Turrini, D., Witasse, O., 2020. A Review of the in Situ Probe Designs from Recent Ice Giant Mission Concept Studies. *Space Science Reviews* 216, 17. doi:<https://doi.org/10.1007/s11214-020-0639-1>.
- Slipher, V.M., 1904. On the spectra of Neptune and Uranus. *Lowell Observatory Bulletin* 1, 87–90.
- Smith, B.A., Soderblom, L.A., Beebe, R., Bliss, D., Boyce, J.M., Brahic, A., Briggs, G.A., Brown, R.H., Collins, S.A., Cook, A.F., Croft, S.K., Cuzzi, J.N., Danielson, G.E., Davies, M.E., Dowling, T.E., Godfrey, D., Hansen, C.J., Harris, C., Hunt, G.E., Ingersoll, A.P., Johnson, T.V., Krauss, R.J., Masursky, H., Morrison, D., Owen, T., Plescia, J.B., Pollack, J.B., Porco, C.C., Rages, K., Sagan, C., Shoemaker, E.M., Sromovsky, L.A., Stoker, C., Strom, R.G., Suomi, V.E., Synnott, S.P., Terrile, R.J., Thomas, P., Thompson, W.R., Veverka, J., 1986. *Voyager 2 in the Uranian System: Imaging Science Results*. *Science* 233, 43–64. doi:<https://doi.org/10.1126/science.233.4759.43>.
- Smith, M.D., Gierasch, P.J., 1995. Convection in the outer planet atmospheres including ortho-para hydrogen conversion. *Icarus* 116, 159–179. doi:<https://doi.org/10.1006/icar.1995.1118>.
- Soderlund, K.M., Heimpel, M.H., King, E.M., Aurnou, J.M., 2013. Turbulent models of ice giant internal dynamics: Dynamos, heat transfer, and zonal flows. *Icarus* 224, 97–113. doi:<https://doi.org/10.1016/j.icarus.2013.02.014>.
- Soderlund, K.M., Stanley, S., 2020. The underexplored frontier of ice giant dynamos. *Philosophical Transactions of the Royal Society of London Series A* 378, 20190479. doi:<https://doi.org/10.1098/rsta.2019.0479>.
- Sromovsky, L.A., de Pater, I., Fry, P.M., Hammel, H.B., Marcus, P., 2015. High S/N Keck and Gemini AO imaging of Uranus during 2012–2014: New cloud patterns, increasing activity, and improved wind measurements. *Icarus* 258, 192–223. doi:<https://doi.org/10.1016/j.icarus.2015.05.029>, [arXiv:1512.05009](https://arxiv.org/abs/1512.05009).
- Sromovsky, L.A., Fry, P.M., 2005. Dynamics of cloud features on Uranus. *Icarus* 179, 459–484. doi:<https://doi.org/10.1016/j.icarus.2005.07.022>.
- Sromovsky, L.A., Fry, P.M., 2007. Spatially resolved cloud structure on Uranus: Implications of near-IR adaptive optics imaging. *Icarus* 192, 527–557. doi:<https://doi.org/10.1016/j.icarus.2007.07.017>.
- Sromovsky, L.A., Fry, P.M., Hammel, H.B., Ahue, W.M., de Pater, I., Rages, K.A., Showalter, M.R., van Dam, M.A., 2009. Uranus at equinox: Cloud morphology and dynamics. *Icarus* 203, 265–286. doi:<https://doi.org/10.1016/j.icarus.2009.04.015>.
- Sromovsky, L.A., Fry, P.M., Hammel, H.B., de Pater, I., Rages, K.A., 2012. Post-equinox dynamics and polar cloud structure on Uranus. *Icarus* 220, 694–712. doi:<https://doi.org/10.1016/j.icarus.2012.05.029>, [arXiv:1503.00592](https://arxiv.org/abs/1503.00592).

- Sromovsky, L.A., Fry, P.M., Hammel, H.B., de Pater, I., Rages, K.A., Showalter, M.R., 2007. Dynamics, evolution, and structure of Uranus' brightest cloud feature. *Icarus* 192, 558–575. doi:<https://doi.org/10.1016/j.icarus.2007.05.015>.
- Sromovsky, L.A., Karkoschka, E., Fry, P.M., de Pater, I., Hammel, H.B., 2019. The methane distribution and polar brightening on Uranus based on HST/STIS, Keck/NIRC2, and IRTF/SpeX observations through 2015. *Icarus* 317, 266–306. doi:<https://doi.org/10.1016/j.icarus.2018.06.026>, [arXiv:1806.01154](https://arxiv.org/abs/1806.01154).
- Sromovsky, L.A., Karkoschka, E., Fry, P.M., Hammel, H.B., de Pater, I., Rages, K., 2014. Methane depletion in both polar regions of Uranus inferred from HST/STIS and Keck/NIRC2 observations. *Icarus* 238, 137–155. doi:<https://doi.org/10.1016/j.icarus.2014.05.016>, [arXiv:1502.06480](https://arxiv.org/abs/1502.06480).
- Stevenson, D.J., 1986. The Uranus-Neptune Dichotomy: the Role of Giant Impacts, in: Lunar and Planetary Science Conference, pp. 1011–1012.
- Stoker, C.R., Toon, O.B., 1989. Moist convection on Neptune. *Geophys. Res. Lett.* 16, 929–932. doi:<https://doi.org/10.1029/GL016i008p00929>.
- Stratman, P.W., Showman, A.P., Dowling, T.E., Sromovsky, L.A., 2001. EPIC Simulations of Bright Companions to Neptune's Great Dark Spots. *Icarus* 151, 275–285. doi:<https://doi.org/10.1006/icar.2001.6603>.
- Swinyard, B.M., Polehampton, E.T., Hopwood, R., Valtchanov, I., Lu, N., Fulton, T., Benielli, D., Imhof, P., Marchili, N., Baluteau, J.P., Bendo, G.J., Ferlet, M., Griffin, M.J., Lim, T.L., Makiwa, G., Naylor, D.A., Orton, G.S., Papageorgiou, A., Pearson, C.P., Schulz, B., Sidher, S.D., Spencer, L.D., van der Wiel, M.H.D., Wu, R., 2014. Calibration of the Herschel SPIRE Fourier Transform Spectrometer. *Monthly Notices of the Royal Astronomical Society* 440, 3658–3674. doi:<https://doi.org/10.1093/mnras/stu409>, [arXiv:1403.1107](https://arxiv.org/abs/1403.1107).
- Teanby, N.A., Irwin, P.G.J., 2013. An External Origin for Carbon Monoxide on Uranus from Herschel/SPIRE? *ApJ Letters* 775, L49. doi:<https://doi.org/10.1088/2041-8205/775/2/L49>.
- Teanby, N.A., Irwin, P.G.J., Moses, J.I., 2019. Neptune's carbon monoxide profile and phosphine upper limits from Herschel/SPIRE: Implications for interior structure and formation. *Icarus* 319, 86–98. doi:<https://doi.org/10.1016/j.icarus.2018.09.014>.
- Teanby, N.A., Irwin, P.G.J., Moses, J.I., Helled, R., 2020. Neptune and Uranus: ice or rock giants? *Philosophical Transactions of the Royal Society of London Series A* 378, 20190489. doi:<https://doi.org/10.1098/rsta.2019.0489>.
- Thomas, E., Stallard, T., Melin, H., Chowdhury, N., 2020. Searching for Uranus's Infrared Aurorae from NIRSPEC Observations, in: European Planetary Science Congress, pp. EPSC2020–797.
- Tice, D.S., Irwin, P.G.J., Fletcher, L.N., Teanby, N.A., Hurley, J., Orton, G.S., Davis, G.R., 2013. Uranus' cloud particle properties and latitudinal methane variation from IRTF SpeX observations. *Icarus* 223, 684–698. doi:<https://doi.org/10.1016/j.icarus.2013.01.006>.
- Toledo, D., Irwin, P.G.J., Rannou, P., Teanby, N.A., Simon, A.A., Wong, M.H., Orton, G.S., 2019. Constraints on Uranus's haze structure, formation and transport. *Icarus* 333, 1–11. doi:<https://doi.org/10.1016/j.icarus.2019.05.018>.
- Toledo, D., Irwin, P.G.J., Teanby, N.A., Simon, A.A., Wong, M.H., Orton, G.S., 2018. Uranus's Northern Polar Cap in 2014. *Geophys. Res. Lett.* 45, 5329–5335. doi:<https://doi.org/10.1029/2018GL077654>.
- Trafton, L.M., Geballe, T.R., Miller, S., Tennyson, J., Ballester, G.E., 1993. Detection of H<sub>3</sub><sup>+</sup> from Uranus. *ApJ* 405, 761. doi:<https://doi.org/10.1086/172404>.
- Tyler, G.L., Sweetnam, D.N., Anderson, J.D., Campbell, J.K., Eshleman, V.R., Hinson, D.P., Levy, G.S., Lindal, G.F., Marouf, E.A., Simpson, R.A., 1986. Voyager 2 Radio Science Observations of the Uranian System: Atmosphere, Rings, and Satellites. *Science* 233, 79–84. doi:<https://doi.org/10.1126/science.233.4759.79>.
- Venot, O., Cavalié, T., Bounaceur, R., Tremblin, P., Brouillard, L., Lhoussaine Ben Brahim, R., 2020. New chemical scheme for giant planet thermochemistry. Update of the methanol chemistry and new reduced chemical scheme. *Astron. Astrophys* 634, A78. doi:<https://doi.org/10.1051/0004-6361/201936697>, [arXiv:1912.07246](https://arxiv.org/abs/1912.07246).
- Visscher, C., Fegley, B.J., 2005. Chemical Constraints on the Water and Total Oxygen Abundances in the Deep Atmosphere of Saturn. *Astrophys. J.* 623, 1221–1227. doi:<https://doi.org/10.1086/428493>.
- Wakeford, H.R., Dalba, P.A., 2020. The exoplanet perspective on future ice giant exploration. *Philosophical Transactions of the Royal Society of London Series A* 378, 20200054. doi:<https://doi.org/10.1098/rsta.2020.0054>, [arXiv:2007.02651](https://arxiv.org/abs/2007.02651).
- Weidenschilling, S.J., Lewis, J.S., 1973. Atmospheric and cloud structures of the jovian planets. *Icarus* 20, 465–476.

- Wildt, R., 1932. Methan in den Atmosphären der großen Planeten. *Naturwissenschaften* 20, 851–851.  
doi:<https://doi.org/10.1007/BF01504582>.
- Wilson, H.F., Wong, M.L., Militzer, B., 2013. Superionic to Superionic Phase Change in Water: Consequences for the Interiors of Uranus and Neptune. *Physical Review Letters* 110, 151102.  
doi:<https://doi.org/10.1103/PhysRevLett.110.151102>,  
[arXiv:1211.6482](https://arxiv.org/abs/1211.6482).
- Young, C.A., 1883. The ellipticity and Surface-markings of Uranus. *Astronomische Nachrichten* 107, 9.  
doi:<https://doi.org/10.1002/asna.18841070103>.
- Zarka, P., Pedersen, B.M., 1986. Radio detection of Uranian lightning by Voyager 2. *Nature* 323, 605–608.  
doi:<https://doi.org/10.1038/323605a0>.